AN APPROACH TO DRAG REDUCTION
IN HIGH SPEED SURFACE VESSELS

A Thesis

Submitted to the Graduate Faculty of the
University of New Orleans
in partial fulfillment of the
requirements for the degree of

Master of Science
in
The Naval Architecture and Marine Engineering Program

by

Kenneth J. Maloney

B.S., University of New Orleans, 1998

May 2002

This work is dedicated to my wife, best friend and the love of my life, Jennifer.

It would not have been possible without her support.

T.T.T.

Put up in a place

where it's easy to see

the cryptic admonishment

T.T.T.

When you feel how depressingly

slowly you climb,

it's well to remember that

Things Take Time.

Piet Hein

ACKNOWLEDGEMENT

that Dr. Bishop's fateful words: "Well Mr. Maloney, you can start over again, or not at all." would have led to this thesis, almost 11 years after they were spoken on the 9th floor of the Engineering Building?

Finally, I cannot thank my family enough for all that they have done for me. Their sacrifices, contributions and love have been the keys to my success.

TABLE OF CONTENTS

LIST OF TABLES

LIST OF FIGURES

NOTATION

The following list of variables and symbols is provided as a quick reference for the reader. These symbols are used in the text and formulas in this document. Symbols (variables) used in the computer programs provided in the Appendices are defined in the variable lists at the beginning of each program or subroutine.

AR	Aspect ratio, wing span^2 divided by its plan form area.
C	Wing section camber (= $0.0679C_{LW}$).
C_{Di}	Induced drag coefficient.
C_f	Viscous friction coefficient
C_L	Two dimensional lift coefficient
C_{Ld}	Two dimensional design lift coefficient at zero angle of attack
C_{Lw}	Lift coefficient for a three-dimensional wing or foil
d	Depth below the free surface measured in chords
D	Drag
D_E	Effective drag.
F_1	Forces in the longitudinal (fore/aft) direction
F_3	Forces in the vertical direction
F_5	Moments about the transverse axis
Fn	Froude number
Fn_D	Design Froude number.
g	Acceleration of gravity

h	Height of the water column above the foil
I_{55}	Moment of inertia about the pitch axis
l	Design waterline length
L	Lift or total lift
L/D	Lift to drag ratio
L_B	Buoyant lift
L_D	Dynamic lift
L_T	Total lift, $(L_D + L_B)$
m	Mass of the vessel
P_{Atm}	Atmospheric pressure
P_{Hyd}	Hydrostatic pressure
P_L	Lift system power
P_{Vap}	Vapor pressure of water
r_i	Radius
Rn	Reynolds number
S	Plan form area of a wing. Also - total wetted surface area
t_B	Brocket optimum foil thickness ratio (maximum thickness/chord)
U	Velocity
Xc	Longitudinal center of gravity
Zc	Vertical center of gravity
α	Angle of attack (radians)
α_i	Ideal angle of attack (radians)

ρ	Density of water
ν	Kinematic viscosity of water
Γ	Gammah, circulation
σ	Cavitation number
∇	Displaced volume of the hull
$\ddot{\eta}_i$	Accelerations, surge: i=1, heave: i=3, pitch: i=5
$\hat{q}_{1,2}$	Induced velocity vector
$\hat{r}_i$	Unit vector
$\%C_{Di}$	Percentage of the infinite depth induced drag coefficient
$\%C_L$	Percentage of the infinite depth lift coefficient

ABSTRACT

Numerous methods for reducing high-speed surface ship drag have been studied by researchers in the fields of naval architecture and marine engineering. Drag alone however, is not the only measure of merit used in the evaluation of a practical design. Accordingly, the ratio of total ship weight versus drag (lift/drag or L/D) is used in this paper to assess the comparative practicality of various designs. The typical methods used to reduce drag in surface ships have focused primarily on reducing wave making drag by either increasing waterline length or decreasing the waterplane area. This thesis explores an alternate method for reducing drag by minimizing both wave making and viscous friction through the substitution of lesser quantities of lift induced drag. This is accomplished with the use of hydrofoils, which lift the ship's hull out of the water, decreasing both viscous and wave making drag. At the design point, the drag of high-speed vessels can be significantly reduced by using this approach. An evaluation of hybrid hydrofoil performance and design issues is provided along with the methods and computer codes used to verify the hypothesis. A theory for predicting the rough order of magnitude of the maximum lift/drag ratios of various types of surface vessels, including slender mono-hulls, air cushion vessels, surface effect ships and hydrofoils is also explored.

INTRODUCTION

The primary purpose of this work is to develop a high-speed surface vessel that requires less thrust to achieve its design speed than is currently required by existing designs. This objective, while sounding simple, involves a delicate balance between a number of factors including sea keeping, maneuvering, arrangements, manufacturability and maintainability. Therefore, the secondary objective of this thesis is to develop a concept that not only shows significant reductions in drag, but also does it without making sacrifices in areas that are important to the owner, user, and builder.

Since drag varies widely with the speed and size of ships, a non-dimensional approach should be use in developing the basic theories. This enables the results to be scaled to any size vessel. Four key variables are used in this non-dimensional approach; the weight of the vessel (lift), its resistance (drag), speed and waterline length. Lift and drag can be combined and nondimensionalized as the ratio of lift divided by drag, or L/D. Speed and length can be combined in a nondimensional form by converting them to a Froude number. Once the data for a given vessel is nondimensionalized, valid comparisons can be made between ships of different sizes and configurations.

Various classifications have been developed for the myriad of ship designs that have emerged over the centuries, but these are normally based on the form or function of the ship. In this study, three basic classes of vessels will be studied and they are defined not by form or function, but by their means of generating lift. Until the last century, all vessels fell into one of these classes, the gravity or displacement class. This type of ves-

sel relies on Archimedes' principal to generate lift from buoyancy. At this time, two other classes of support are possible. These classes use powered and dynamic lift respectively.

Ships that employ only buoyant lift suffer two main forms of drag, viscous friction drag and wave making drag, which can be further subdivided into transverse and divergent wave drag. Many different types of displacement vessels have been developed to reduce buoyancy related drag. These forms have primarily focused on reducing wave making drag and many employ increased wetted surface areas, essentially trading incremental increases in viscous drag for more significant reductions in wave drag.

Powered lift is the type of lift used by air cushion vessels. This class of vessel generates a cavity of pressurized air under its hull that lifts it out of the water, nearly eliminating wetted surfaces. Air cushion vessels experience significantly reduced viscous friction drag but still suffer from wave making drag. Additionally, the pressurized air volume must be generated by an independent power source. This power source effectively generates a drag "tax" on the vessel, which is present at all speeds, because it cannot achieve its low-drag performance without paying this continuous power penalty. This effective drag must be considered when evaluating the L/D of air cushion vessels.

Dynamic lift can be produced by hydrofoils or lifting surfaces located above or below the water surface. This lift is a result of a pressure differential created between the upper and lower sides of the lifting surfaces, according to Bernoulli's principle, and is proportional to the velocity squared. As with powered lift, dynamic lift has its own unique drag penalty, induced drag.

When comparing the various forms of lift and their associated drag, the one that produces the best L/D depends on the speed at which the comparison is made and the length of the vessel. Buoyant lift produces significantly higher L/Ds at low speeds. Air cushion vessels produce their best results at high speeds, while lifting surfaces have nearly constant L/D ratios at all speeds.

In addition to the three basic classes of craft, a spectrum of hybrids can be developed. A hybrid, as defined in this work, is a vessel that employs more than one form of lift. All hybrids must rely on buoyancy as a primary means of support for safety reasons. It would be both impractical and inconvenient to have air cushion vessel or hydrofoil sink to the bottom every time it shut down its power plant. Therefore, air cushion vessels and hydrofoils must be designed to be hybrids, or be capable of floating when powered down.

This work was undertaken to investigate the hypothesis that a high speed hybrid that employs both buoyant and dynamic lift can develop significantly higher lift to drag ratios than vessels supported by buoyancy alone. To test this theory, the lift and drag characteristics of an optimal displacement hull form were combined with those of an optimized lifting surface to create a hybrid hydrofoil.

The first step in developing proof of this hypothesis was an exploration of the lift to drag ratios of the three classes of vessels and the factors that govern their performance. Semi-empirical relationships were then developed to predict maximum lift to drag ratios of the pure classes of vessels and for the hybrids. The hybrid hydrofoil was selected for development and a design Froude number of 1.0 was chosen. Computer programs were then used to develop the hybrid and predict its performance.

1 - LIFT/DRAG RATIOS OF HIGH SPEED SURFACE VESSELS

In this section, a comparison of the lift to drag (L/D) ratios for a number of designs employing the three basic types of lift will be presented. The data used in this study was obtained from model tests conducted in calm water. There were two reasons for undertaking a study of model test data. The primary reason was to set a performance objective for a new hybrid. The second reason was to identify an efficient displacement hull form to provide buoyant lift for the ship.

Upon analysis, it was found that distinct patterns in the plots of the L/D data could be associated with the different types of vessels used in the study. A theoretical explanation for these characteristic shapes was then developed and subsequently used to justify the selection of the performance objectives for the hybrid.

1.1 - A Characterization of "High Speed"

The title of this thesis uses the term "high speed." Since the term has comparative connotations, it requires proper characterization as it applies to this work. For example, "high speed" is well over 100 knots when referring to an offshore racing boat. In general, the object of this thesis is to produce a practical vessel that can either be employed in commercial or military service. In that context, 50 knots fit the definition of "high speed" very well and was subsequently used as the upper target velocity for the hybrid vessel. Likewise, an offshore racer hardly meets the requirements for a practical design, unless it is intended for racing.

There are a number of pragmatic reasons for limiting design speeds to 50 knots as well. Since the analysis deals strictly with hydrodynamics, the speeds should be kept below a point where the resistance is not affected significantly by aerodynamic drag. In order to keep this presumption valid, speeds should be limited to a maximum of 50 knots. Another factor that is important in setting a 50 knot limit is the potential for cavitation on the foil surfaces. Speeds should be kept below the point where cavitation inception was likely. Again, a speed of 50 knots is the most likely maximum.

1.2 - A Survey of Model Test Data

Data from a number of model tests was used in the initial investigations of this project. This data was obtained from several sources, including the Society of Naval Architects and Marine Engineers, the U.S. Navy, the U.S. Coast Guard, and Textron Marine & Land Systems. It includes tests of displacement mono-hulls, planing mono-hulls and a surface effect ship.

The study was begun by reducing all resistance data to L/D format. This was accomplished by dividing the displacement of the hull during the test by the total measured resistance at each speed. The data was further nondimensionalized by converting test speeds to equivalent Froude numbers as shown in Equation 1.

$$Fn = \frac{U}{\sqrt{gl}}$$
(1)

Where: Fn = Froude number

           U = velocity

g = acceleration of gravity

l = length of the hull at the design waterline.

The first model tests analyzed for this study were the Series 64, slender displacement mono-hulls.[14] The hulls had round bilges and transom, sterns with minimal transom emersion. These tests systematically varied a number of parameters, including block coefficient, length/draft ratio and length/beam ratio. A sampling of tests for six of the 15 test models conducted in the series is presented in Figure 1. The relationship between these models is readily apparent, as indicated by the tight grouping of the data.
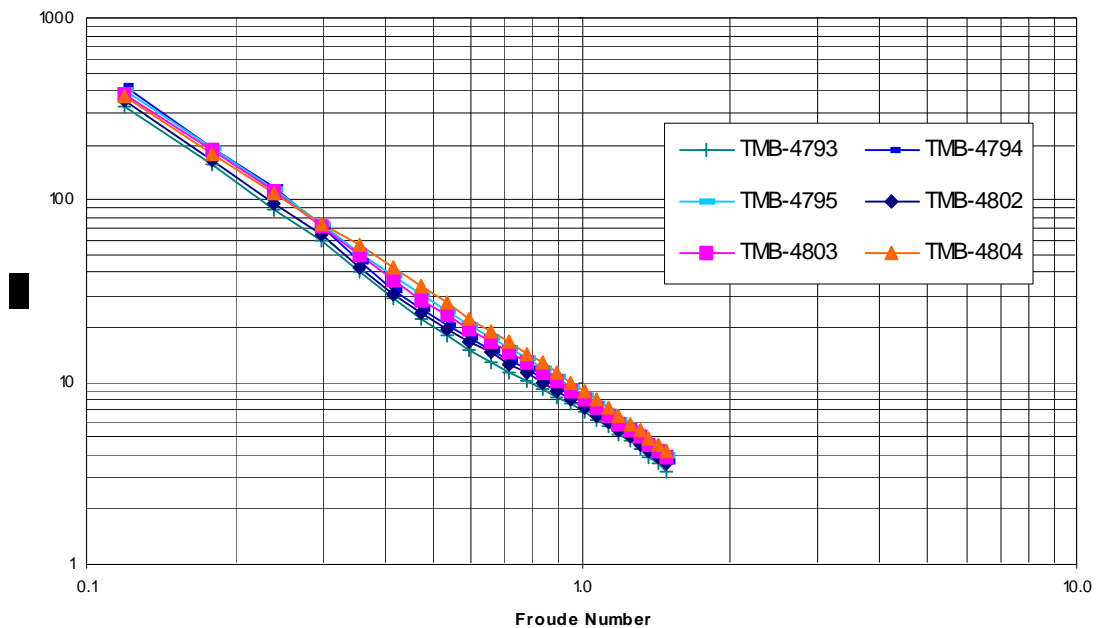
Figure 1   Lift/Drag ratios for Series 64 slender displacement mono-hulls.

The next model tests analyzed were the Series 62, planing mono-hulls.[4] These tests were conducted on five hard chine planing models which all had similar body plans (sections). The lengths of the models were systematically altered to yield a series that

varied primarily in length/beam ratio. Each model was also tested at three different dis-

placements and each displacement condition was tested with multiple longitudinal centers

of gravity. A plot of selected tests is shown in Figure 2. As with the Series 64 models, a

close relationship can be seen in the data.
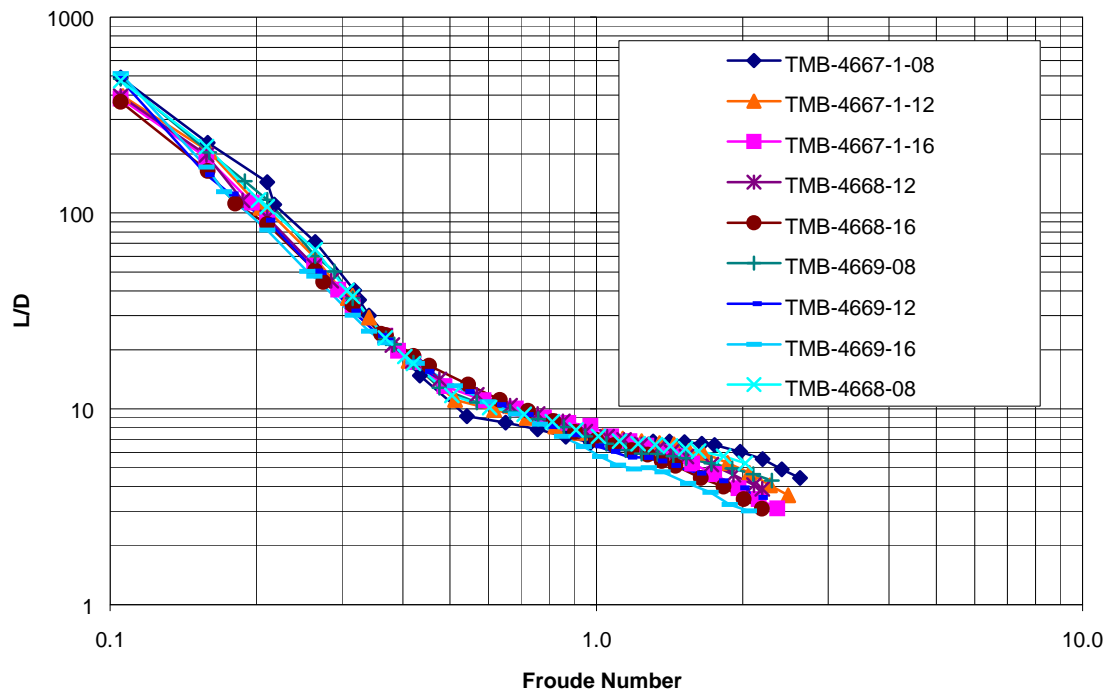
Figure 2   Lift/Drag ratios for Series 62 planing mono-hulls.

Under the hull type classification system used in this thesis, the planing mono-

hull must be considered a hybrid because it employs both buoyant and dynamic lift. At

low speeds, the hull is supported strictly by buoyancy. As speed increases, the hull bot-

tom, which is designed to generate dynamic lift, assumes a greater and greater portion of

the lifting function. The bottom can be classified as a ventilated lifting surface, which is

a special case for hydrofoils.

The last group of model tests reviewed was a collection of hybrid designs. This collection [15] includes an inverted "V" planing hull known as a Hickman Sea Sled. Although this hull form is radically different from other planing hulls, it is nonetheless a hybrid, combining dynamic lifting surfaces with a displacement hull. The data shown in Figure 3 is very similar to that of the Series 62 planing hulls, including the characteristic "dog leg". Figure 3 also includes test data from the USCG 47-foot Motor Lifeboat, which is a planing mono-hull with built-in trimming wedges at the stern. It too has a L/D curve similar to the Series 62 hulls.
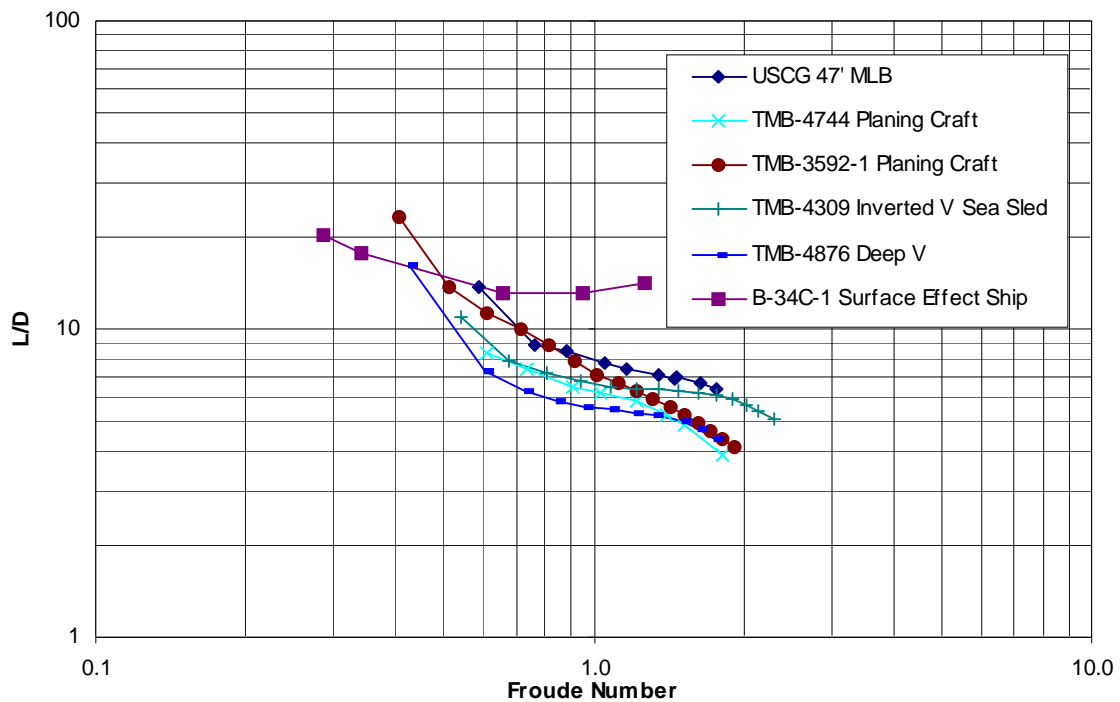
Figure 3   Lift/Drag ratios of various model tests.

Another hybrid is included in the Figure 3. It is the B-34C-1 surface effect ship, also known as the Bell-Halter BH-110. A surface effect ship is a hybrid vessel that uses a

pressurized air cushion in combination with a catamaran hull to generate lift. The BH-110 can actually be considered a triple hybrid because the catamaran hulls used were hard chine planing hulls. The BH-110 is the only model test data that could be obtained for a hybrid utilizing powered lift. In order to accurately represent the L/D of the SES, the lift fan power was converted to a drag force and added to the model's resistance. Equation 2 was used to convert lift fan power to effective drag.

$$D_e = \frac{P_L}{U}$$ (2)

Where: P_L = lift system power

De = effective drag.

After reviewing this data, the primary design objectives for the new hybrid were determined. A lift to drag ratio of at least 20 at a Froude number of 1.0 would be a significant improvement over the hull forms reviewed. Achieving this objective would require a hull that retained or increased its efficiency as speed increased. The only vessel that exhibited this quality was the surface effect ship. Due it its poor performance at lower speeds and other more practical reasons,[1] it was not chosen as the baseline hull for the hybrid.

The planing mono-hulls, which have typically been used as the buoyant platforms for hydrofoil craft also showed poor L/D characteristics at both low and high speeds. Of

---

[1] The SES vessel type is subject to high operating expenses due to air cushion seal maintenance costs, and a more practical solution was sought in this work.

the planing hulls reviewed, most did not show superior performance characteristics over the displacement types until they exceeded a Froude number of 1.0. Subsequently, the planing mono-hull was not considered as the source of buoyant lift for this project.

Based on the model test data alone, the hull form that could provide the best starting point for the design of a hybrid would be a slender mono-hull similar to those used in the Series 64 tests. The slender mono-hulls maintained the highest L/Ds up to a Froude number of 0.6 and were only surpassed by the SES at this point. As mentioned earlier, they remain superior to planing hulls until they reach a Froude number of 1.0. Based upon these findings, the slender mono-hull was tentatively selected to provide the buoyant lift.

1.3 - Lift to Drag Ratios of Ideal Surface Vessels

The analysis of the data from the model tests indicated that there should be predictable factors among the classes of vessels. These factors tended to control the shapes of their L/D curves. In an effort to obtain equations for that yield curves similar to the ones obtained from the model test data, several simplifying assumptions were made. In general, these ideal equations focus only on the most significant drag effects associated with each form of lift. By doing this, a "best case" could be determined for each type. Exploring these factors was essential in understanding the requirements and contributions of the hybrid elements and knowing if the target that was set in the previous section was physically feasible. Once the factors governing the major components of vessel drag were understood, the choice of a performance objective could be justified with mathematics, even if they were somewhat empirical in nature.

1.3.1 - Displacement Hull (Buoyant L/D)

The Series 64 data shown in Figure 1 plots in almost straight lines on the log-log axes used. This tends to indicate that there is a strong exponential relationship at work between the Froude number and the lift to drag ratio for these models. Based on this assumption, it was presumed that an equation for the lift to drag ratio for a slender displacement vessel of the form of Equation 3 could be derived. In this equation, "*a*" is the L/D ratio at a Froude number of 1.0, and "*b*" indicates the "slope" of the L/D curve when plotted on log/log axes. To test this theory, some simplifying assumptions were made.

$$\frac{L}{D} \approx aFn^b \tag{3}$$

An ideal displacement vessel is one that is very slender and long. If such a ship were possible, the dominant resistance force that it would experience at high speeds would be generated by viscous friction. As a practical matter, a finite length was assumed, but wave-making drag was ignored as a simplifying assumption. This assumption yielded an equation for the maximum L/D of a displacement vessel, since any added wave making drag would only decrease the L/D. With these assumptions in place, the lift to drag ratio of a displacement hull was developed by calculating the vessel's buoyancy and dividing it by the flat plate viscous friction drag, as shown in Equation 4. According to Newman[10], the use of the viscous drag equation for a flat plate is acceptable as long as the hull form in question is streamlined and has a length to thickness ratio of at least 5.0.

$$\frac{L}{D} \approx \frac{\rho g \nabla}{\dfrac{\rho U^2 S C_f}{2}}$$ (4)

Where: ρ = density of water

∇ = displaced volume of the hull

S = wetted surface area

C_f = viscous friction coefficient given by Equation 5.

$$C_f = \frac{0.075}{(\log_{10} Rn - 2.0)^2}$$ (5)

Where: Rn = Reynolds number.

By ignoring wave-making drag, Equations 4 and 5 could be used to approximate the maximum lift to drag ratio attainable by a displacement hull. In order to generalize and simplify these equations further, some additional assumptions can be made. Rho, g, displaced volume and surface area can all be presumed to be constants throughout the speed range. When the Froude number is substituted for the Reynolds number in equation 4, the equation takes the form of Equation 6.

$$C_f = \frac{0.075}{\left(\log_{10}\left(\dfrac{Fn\sqrt{gl^3}}{v}\right) - 2.0\right)^2}$$ (6)

Where: Fn = Froude number per Equation 1

v = kinematic viscosity of water.

Equation 6 is plotted in Figure 4 with three different waterline lengths. A curve fitting function was used to match the data. The "best fit," as indicated by the R^2 correla-

tion factor, was an exponential function of the form $C_f \approx aFn^b$. The correlation factors for all waterline lengths are excellent (> 0.99) and supported using the equations in the range of Froude numbers plotted. This "best fit" approach is further supported when the origins of equation 6 are considered. Equation 6 is only one of a number of viscous friction coefficient formulas that have been developed over the past hundred years. All of which are based on a "best-fit" to data collected from numerous experiments performed on flat plates.

Rounding the coefficients and exponents derived from Figure 4 yields the alternate and more approximate form of the friction coefficient as a function of Froude Number, $Cf \approx 0.001Fn^{-0.1}$. This is applicable for vessels with waterline lengths ranging in size from 50 to 300 meters.
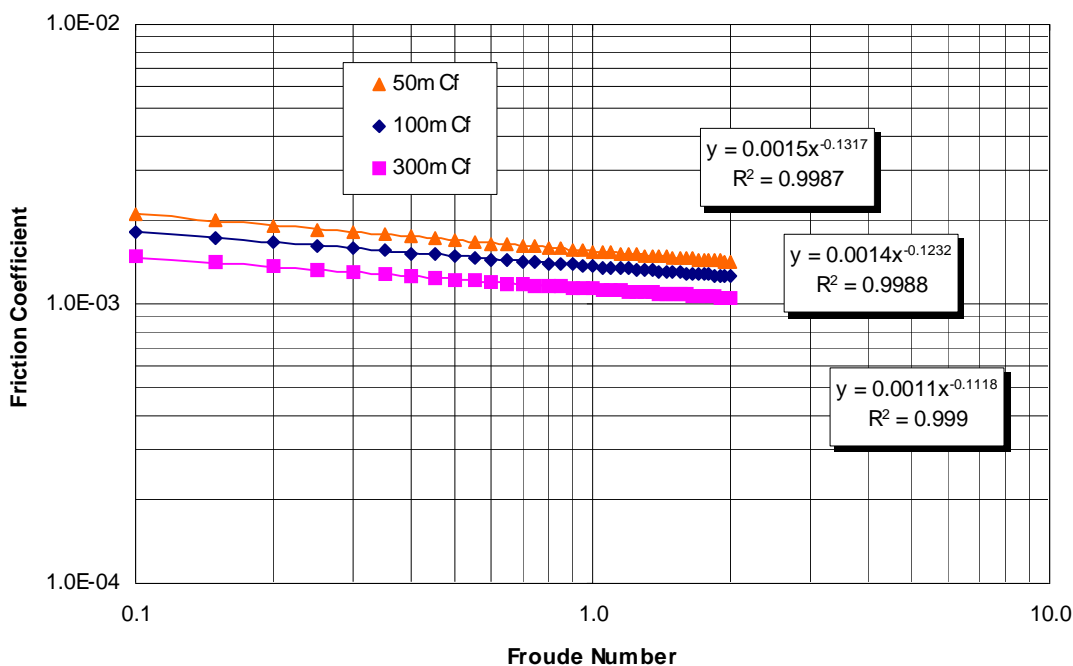
Figure 4 Viscous friction coefficients as a function of Froude number.

The alternate Froude number based form of the friction coefficient can now be substituted for *Cf* in Equation 4. By rearranging the terms of Equation 1, Fn^2gl can be substituted for U^2 into Equation 4 as well. After making these substitutions and canceling terms, the L/D of an ideal surface ship in the range of 50 to 300 meters in length takes the form of Equation 7.

$$\frac{L}{D} \approx \frac{2000\nabla}{lS} Fn^{-1.9} \qquad (7)$$

Equation 7 indicates that the maximum lift to drag ratio of a surface ship is governed primarily by the ratio of its displaced volume to its wetted surface area. It also shows that the L/D can be expressed in the form of Equation 3, since the displaced volume, length and wetted surface area can be assumed to remain constant. Equations 3 and 7 are plotted in Figure 5 along with scaled data for a Series 64 slender mono-hull. Equation 3 has been adjusted to match the data for the model test. The use of Equation 4 in lieu of Equation 7 improves the solution, but there are still significant differences between the test data and the theoretical result. This can be attributed to the exclusion of wave-making resistance from the solution and the fact that Model 4787 does not meet the definition of the "ideal" surface vessel.
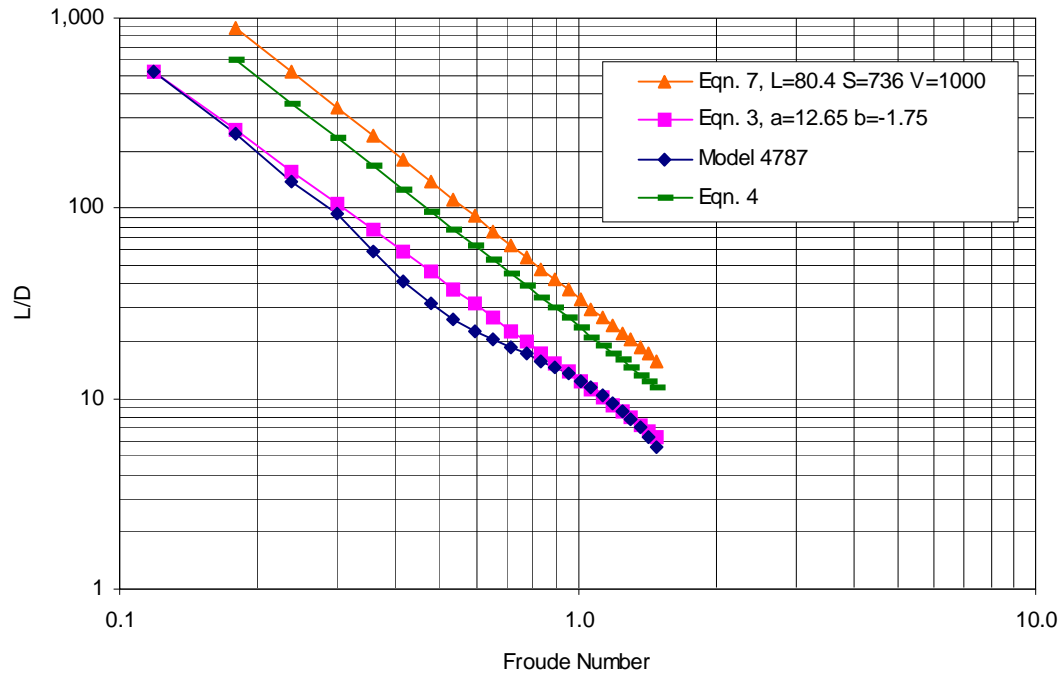
Figure 5   Lift to drag ratio of an ideal surface vessel.

1.3.2 - Lifting Surface (Dynamic L/D)

According to Breslin and Andersen [2], the lift to drag ratio of a three dimension-al wing submerged in a real fluid can be expressed in terms of the lift coefficient (C_L), viscous drag coefficient (Cf) and the aspect ratio (AR) of the wing. This expression is shown in Equation 7, and it applies only to airfoils with aspect ratios greater than four. The lift coefficient is a function of the wing's design and angle of attack. The viscous drag coefficient is a function of the Reynolds number.

$$\frac{L}{D} = \frac{C_L}{\frac{C_L{}^2}{\pi AR} + C_f} \tag{8}$$

Solutions for Equation 8 were developed using Equation 6 to obtain the friction coefficient, with the foil's chord length substituted for l.[2] Figure 6 shows the results of the calculations. The chart indicates that the lift to drag ratio of a lifting surface has a dependence on Froude number as well as aspect ratio. Again, exponential curves were fit to the results, and as seen in the figure, equations of the form of Equation 3 can be obtained with excellent correlation factors. This is an approximation however, as Equation 8 cannot be converted to this form algebraically due to the presence of C_f in the denominator.

---

[2] The Froude numbers calculated for the foils were based on a chord length of 2.0m. This chord Froude number cannot be associated directly with a ship's Froude number and the use of the absolute velocity is recommended when calculating the L/D of a wing that is associated with a ship hull.
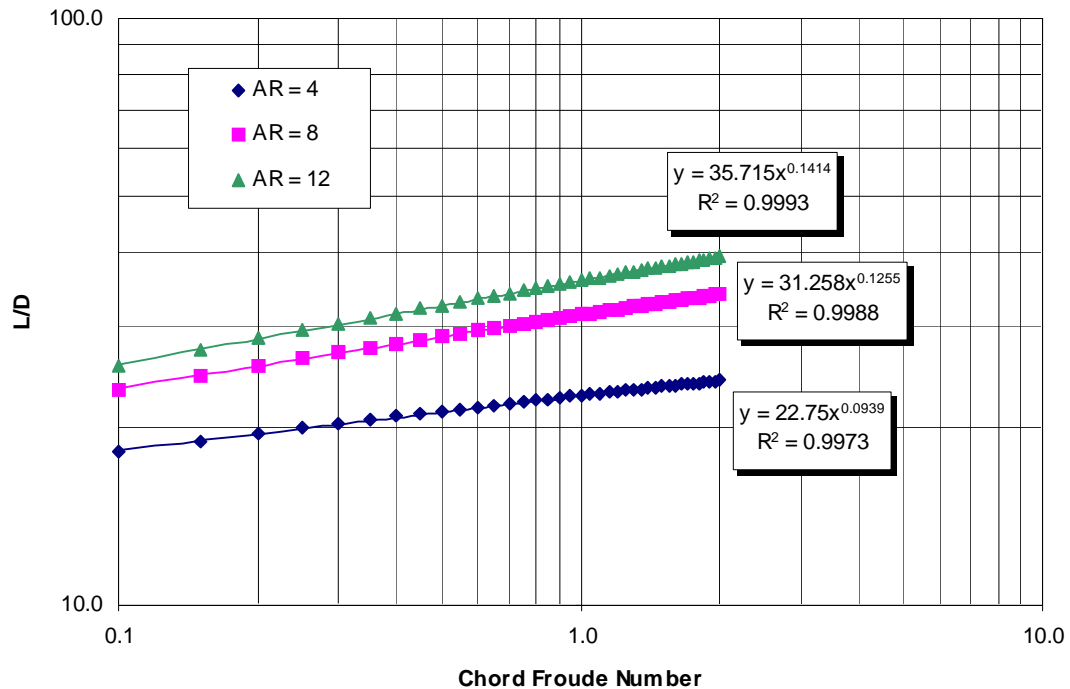
Figure 6   Lift to drag ratio of finite wings in a real fluid.

This formulation for the L/D of a hydrofoil presumes that the foil is completely immersed in an ideal fluid. It also presumes that the fluid is infinitely deep and therefore ignores any wave making drag and free-surface effects. It does however account for the major drag factors associated with wings, induced and viscous friction drag.

1.3.3 - Air Cushion Vessel (Powered L/D)

An ideal air cushion vessel (ACV) is one that has no contact with surface. It would also be able to achieve a hover state without creating an air gap. At speed, this vessel would not create waves. With these simplifying assumptions, the only drag re-maining is the effective drag created by the lift fan engines, as stated in Section 1.2. This

is an obvious oversimplification, since air is continuously leaking from a real ACV. In addition, if it were not in contact with the surface, a gap between the ACV and the water surface would be implied, and leakage would follow. Nonetheless, the assumptions that lift power is a constant and the total airflow through the system is zero, provide the conditions for obtaining the maximum lift to drag ratio possible for a vessel employing this type of lift.

In Section 1.2, the drag of a surface effect ship (SES) model was analyzed. In order to account for the effective drag created by the lift engines, Equation 2 was used. Using Equation 2, the lift to drag ratio of an ideal ACV can be determined. Equation 9 is the basis for the lift to drag ratio of an ideal ACV, which is plotted in Figure 7.

$$\frac{L}{D} \approx \frac{mg}{\left(P_L \middle/ U \right)} \tag{9}$$

Where: m =   Mass of the vessel

P_L =   Lift engine power.
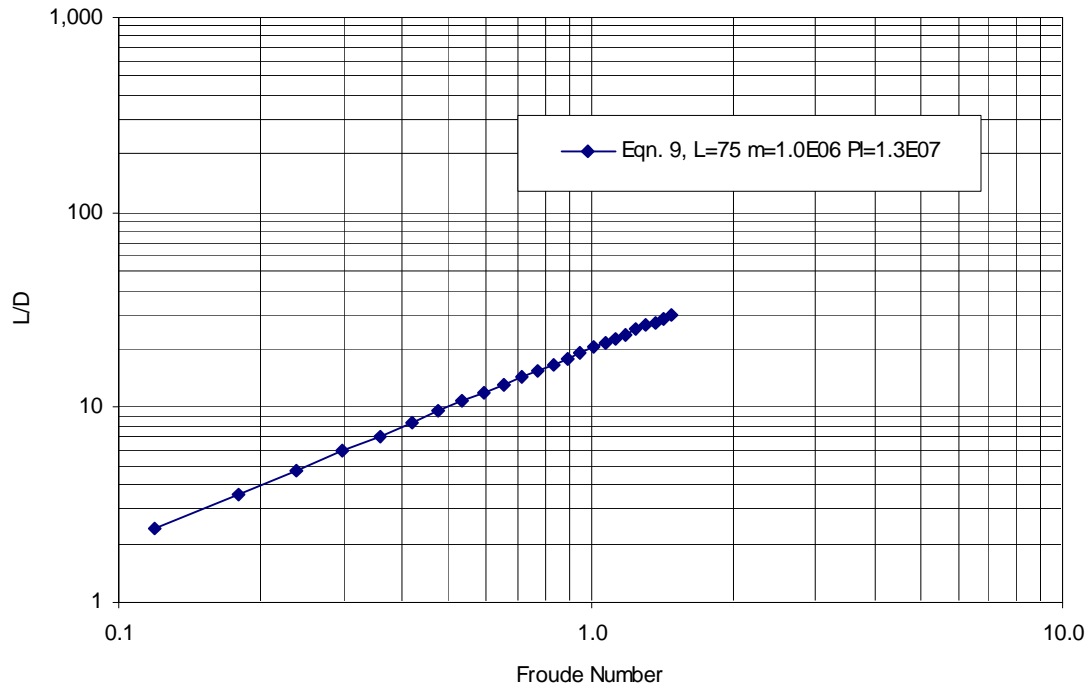
Figure 7   Lift to drag ratio of an ideal air cushion vessel.

As an ideal ACV, further simplifying assumptions can be made that presume both weight and power are constant and independent of velocity. If the velocity term in Equation 9 is expressed in terms of the Froude number and the terms are rearranged, Equation 9 takes the form of Equation 10.

$$\frac{L}{D} \approx \frac{m\sqrt{g^3 l}}{P_L} Fn \tag{10}$$

In Equation 10, m, g, l and P_L either are constants or presumed to be constant. As such, Equation 10 is of the form of Equation 3, where $b = 1.0$.

1.4 - Lift to Drag Ratios of Ideal Hybrid Forms

In the previous section, it was demonstrated that the dominant drag functions could be used to develop maximum lift to drag equations for each of the ideal vessels proposed in this thesis. Equations 4, 8 and 9 were used to show that the L/D for each of the ideal types of ships could be resolved into the form of Equation 3. In each of the three types however, different factors are significant. For buoyant lift, hull geometry and wetted surface area are dominant. For dynamic lift, the lift coefficient and aspect ratio are of primary importance. With powered lift, the lift system's efficiency is of primary concern.

1.4.1 - Hybrid Air Cushion Vessel

The most elementary hybrid L/D equation is one that involves a combination of buoyant and powered lift. Hybrids of this type are commonly referred to as surface effect ships (SES). The contributions of the two types of lift can be assumed to be independent of velocity, therefore the L/D equation is the sum of the contributions of the two pure L/D equations in the ratios that the two types of lift share the load. If the vessel is de-signed with 15% buoyant lift and 85% powered lift, that ratio will remain constant throughout the range of speeds for the vessel. Combining equations 7 and 10 at a ratio of 0.15 to 0.85 respectively, an equation for the L/D of an SES can be developed.

$$\frac{L}{D} \approx \left(\frac{2000 \nabla_{0.15}}{lS} Fn^{-1.9} \right) + \left(\frac{0.85 m \sqrt{g^3 l}}{P_L} Fn \right) \tag{11}$$

Where: $\nabla_{0.15}$ = Displaced volume resulting from 15% of the mass of the vessel

l = Length of the side hulls

S = Wetted surface area of the side hulls

m = Total mass of the craft.

Figure 8 shows results derived from Equations 11, 10 and 7. It can be seen that the hybrid ACV, or surface effect ship, is less efficient than a displacement vessel at lower Froude Numbers, but excels at the higher speeds. It also shows that the SES is superior to the pure ACV only at the lower speeds. Data from the B-34C-1 SES model test that was reviewed in section 1.1 is also plotted. The similarity in the shape of the L/D curves indicates that the assumptions that led to the development of Equation 11 have a basis for validity, and that the equation will yield reasonably accurate results.
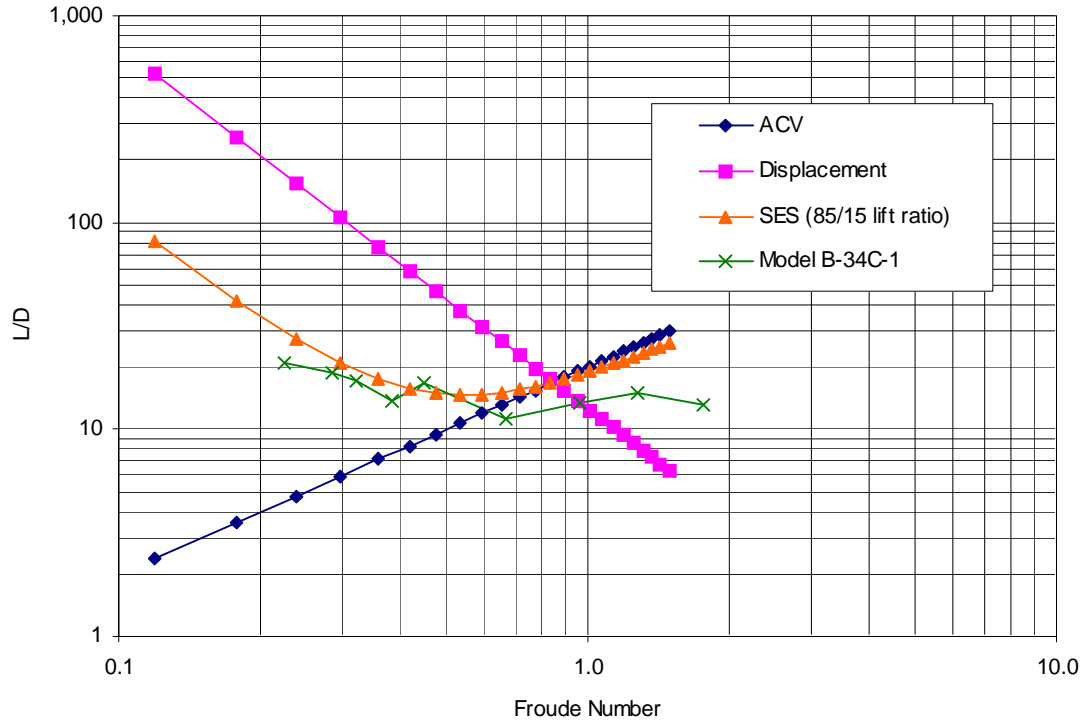
Figure 8   Lift to drag ratio of a surface effect ship.

1.4.2 - Hybrid Hydrofoil

The derivation of an equation for a hybrid employing buoyant and dynamic lift is complicated by the relationship between the two lifting forces, which is a function of velocity. In order to simplify the derivation, the assumption is made that the waterline length of the displacement hull remains constant throughout the transition from fully buoyant support to dynamic support. The dynamic lift developed by a hydrofoil can be expressed in terms of the Froude Number as shown in Equation 12.

$$L_D = \frac{\rho}{2} Fn^2 glSC_L \tag{12}$$

Where: L_D = Dynamic lift

l = Length of the ship

S = Surface area of the hydrofoil

C_L = Lift coefficient.

At any given speed, the total lift (L_T) is equal to the total weight of the craft. This can be expressed as the sum of the buoyant lift (L_B) and the dynamic lift (L_D). To develop an equation for the lift to drag ration of a hybrid hydrofoil, the L/D contributions of each form of lift must be combined proportionally. An equation for the hybrid hydrofoil's lift to drag ratio can be developed from Equation 3, resulting in the hybrid sum shown in Equation 13.

$$\frac{L}{D} \approx \left(\frac{L_T - L_D}{L_T} \right) aFn^b + \left(\frac{L_D}{L_T} \right) cFn^d \tag{13}$$

Where: aFn^b = Lift to drag function for the buoyant lift

cFn^d = Lift to drag function for the dynamic lift

$L = L_T = L_D + L_B$, Total lift

This equation relies on a number of assumptions. Foremost among them is that the L/D relationships aFn^b and cFn^d remain valid as the load shifts from buoyant support to dynamic support. Additional assumptions must be made if a speed dependent relationship between the dynamic and buoyant lift contributions is to be determined. The first assumption is that the lift coefficient will remain constant at all speeds. The second is that the relationship developed in Equation 13 is valid only for Froude Numbers less than or equal to the Froude Number at which the entire weight of the vessel is supported by dynamic lift . If the constant C_L assumption is maintained, Equation 13 becomes invalid at speeds greater than the design Froude Number (Fn_D) because the foil system will generate a lift force that exceeds the weight of the vessel, invalidating the buoyant lift terms. These parameters can be substituted into Equation 12 to define the maximum or design dynamic lift as:

$$L_T = \frac{\rho}{2}\left(Fn_D\right)^2 glSC_L \qquad (14)$$

Where: Fn_D = Design Froude Number.

After substituting Equations 12 and 14 into Equation 13 and rearranging terms, the maximum lift to drag ratio for a hybrid hydrofoil can be expressed in the form of Equation 15.

$$\frac{L}{D} \approx aFn^b + \frac{Fn^2}{Fn_D^2}\left[cFn^d - aFn^b\right] \qquad (15)$$

Figure 9 shows the results of Equations 15, 10 and 8. A design Froude Number of 1.0 was selected. The hybrid has a slightly lower lift to drag ratio than the displacement hull at Froude numbers less than 0.6. This is due to the increased surface area below the waterline. L/D decreases until the point where the dynamic and buoyant lift are equal. From this speed up to the design Froude Number, the L/D increases until it reaches the value of the pure hydrofoil. At this point, it is presumed that the hull has left the water entirely, but the lifting surface is still deeply submerged. This is the point at which the previous assumptions limit further calculation. If higher speeds are to be obtained, the lift coefficient must be decreased in proportion the Fn^2 in order to maintain a constant value for the dynamic lift. As stated earlier, if the lift coefficient is held constant at speeds greater than the design speed, the foil will broach the free surface of the water.
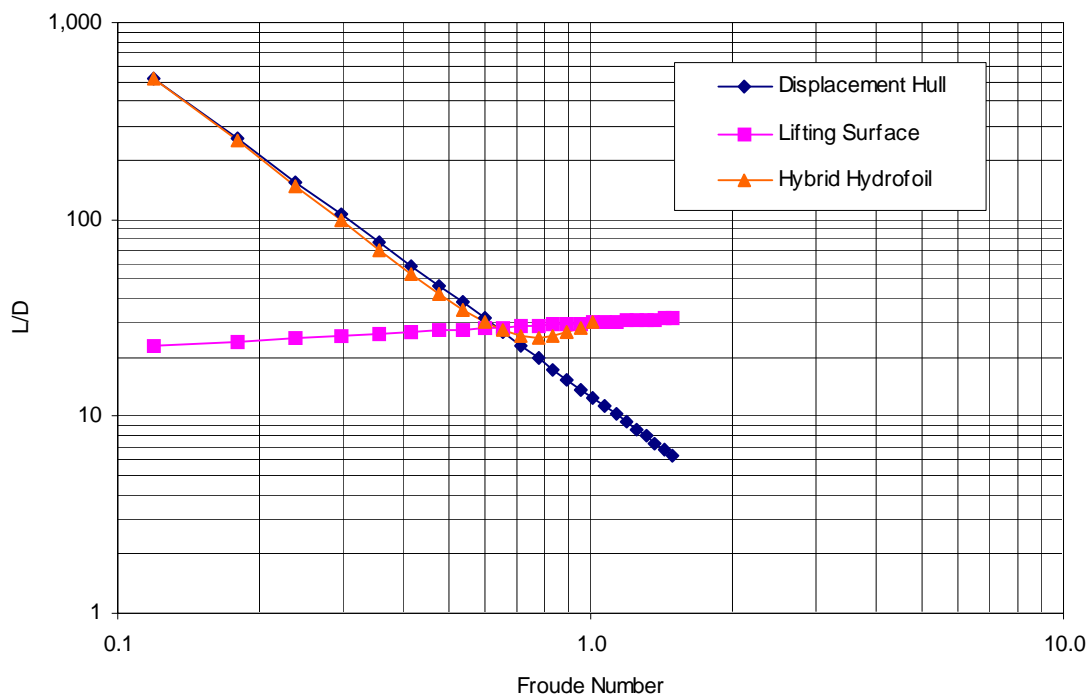
Figure 9   Lift to drag ratio of a hybrid hydrofoil.

Equation 15 indicates that the ability to reach the performance objective set in previous sections relies primarily on the efficiency and design of the lifting surface. Obviously, the hull used in this effort must also have good drag characteristics. If it does not, the propulsion system may not be able to produce enough thrust to reach the speeds necessary for the craft to take advantage of foilborne operation.

2 - OPTIMUM HULL FORM SELECTION

The analysis undertaken in Section 1 used the concept of an "ideal displacement vessel." However, after that analysis was completed, the form of this ideal hull had not been determined. In fact, the ideal displacement hull had a very unusual characteristic. It produced no surface waves. Although the L/D curves for the Series 64 slender mono-hulls were very similar to those of the ideal craft, it could not be presumed that they would offer the best resistance characteristics for the hybrid hydrofoil. In order to meet the overall objectives, a detailed analysis of the drag characteristics of several different types of displacement vessels was necessary.

2.1 - Theoretical Optimum Hull Form

The theory of operation that is proposed for the hybrid hydrofoil is one that supe-rimposes the dynamic lift generated by a lifting surface over the buoyant lift generated by a displacement hull. This design theory deviates from previous hydrofoil designs, which typically used planing hulls for the buoyant portion of their lift. The model tests that were reviewed in Section 1 indicated that most planing hull forms do not achieve the lift to drag efficiency of a slender displacement hull until they reach Froude numbers greater than 1.0. Since the objective of this thesis is to develop a craft that operates at this Froude Number, it is essential to use a hull that maintains high lift to drag ratios for as much of the speed regime as possible. This minimizes the typical drag "hump" asso-ciated with many high performance designs.

In addition to having superior drag characteristics up to a Froude Number of 1.0, the estimation of drag for a displacement vessel is much more straightforward than it is for a planing design. The technology to accurately predict planing hull drag from a standstill up through the full planing regime was not available in the public domain at the time of the study.

The calculation of the drag for the hybrid hydrofoil relies on the theory that a simple superposition of drag calculations can be achieved and the two calculations can be made independently. This process would involve calculating the total resistance of the hull, then the lifting surfaces, and combining the results. The ideal hull form for this application would not only have to possess superior drag characteristics at the design displacement, but be able to maintain these characteristics and smoothly transition to a zero drag condition as it rises out of the water. This would tend to suggest that the winning candidate be a slender, nearly wall sided hull with a rounded bottom similar to those tested in the Series 64 group. This criterion would tend to rule out any discontinuous hull forms, like the small waterplane area twin hull (SWATH) designs. The remaining choices for the parent hull subsequently would be slender mono-hulls, catamarans and trimarans.

The main objective of this effort is to produce a practical design that has commercial as well as military applications. As stated previously, the slender mono-hull (SMH) is well suited primarily for combatant service due to its limited stability. This leaves the real choices for the parent hull to be between a catamaran and a trimaran. The trimaran considered in this case would consist of a slender center hull with two minimal displace-

ment outriggers or amas. The amas would be raised from the water by the lifting surfaces at relatively low speeds, leaving only the slender center hull to provide buoyant lift.

From a practical standpoint, both types of vessels are very attractive. Each lends itself well to layouts with large deck areas and convenient arrangements. In spite of these prejudices, all of the hull types mentioned, including the SWATH, were considered during the analysis.

2.2 - Analysis of Displacement Hull Drag Characteristics

This project began with a search for model test data that could be used to develop the new hull form. The data that was researched however did not include model tests of trimarans or catamarans. There are also no proven methods for combining mono-hull data to accurately estimate multi-hull resistance, since interference between the hulls can be significant at certain speeds. This interference factor can be beneficial or adverse and a proper analysis of a multi-hull design requires not only an analysis of the individual hull characteristics, but of the overall characteristics of the ensemble.

Due to the large number of variables involved with each hull form to be investigated, a computational tool was needed to assist in finding an analytically optimum solution. The first choice was to develop a numerical code for predicting the resistance of displacement hulls. After researching a number of works on panel methods and the work of Kelvin, Michell, Havelock and others, it became apparent that an existing program had to be found for this project. Completion would have been severely delayed by including the development time required for creating such software.

The search for viable software was resolved with the discovery of Michlet, a program written by an Australian researcher named Leo Lazauskas. Lazauskas, working with E.O. Tuck at the University of Adelaide, developed this program, which solves Michell's Integral [9] for surface ships. It simulates the hull's presence with a distribution of Havelock sources [5] on its centerline plane, making it well suited for work with slender hull forms. Michlet also computes the viscous drag based on wetted surface area and for multi-hull vessels, it calculates interference forces as well.

Data input to Michlet consists of a table of offsets for each hull to be analyzed and a single parameter file that contains hull specific information and global settings. Output consists resistance or free surface elevation data in text format as well as "pcx" images of wave patterns at specific speeds. [7]

Tuck [11] introduced a number of mathematical refinements to reduce calculation times, drawing on the work of Newman. The resulting code efficiently calculates the resistance of slender surface vessels on a desktop computer. Michlet's development and the results of calculations made with it have been documented in a number of published reports.

2.2.1 - HullGen, parametric hull form generation computer program

In order to systematically evaluate the large number of hull variations envisioned for this project, a parametric hull description algorithm was devised. It consisted of a series of equations that described the keel heights, waterline half-breadths and transverse section shape of the parametric hull. The algorithm was used to generate tables of offsets that were analyzed with Michlet.

Two different waterline types were investigated. The first waterline, shown in Figure 10, was a simple parabolic waterline that could be altered to allow for a transom or canoe shaped stern. The second, shown in Figure 11, was a more complex shape that combined an ellipse forward with a parabola aft. The intersection point between the two elements is continuous down to the second derivative of each equation, resulting in a mathematically fair waterline. It too could be varied to allow for variations between transom and canoe type sterns.
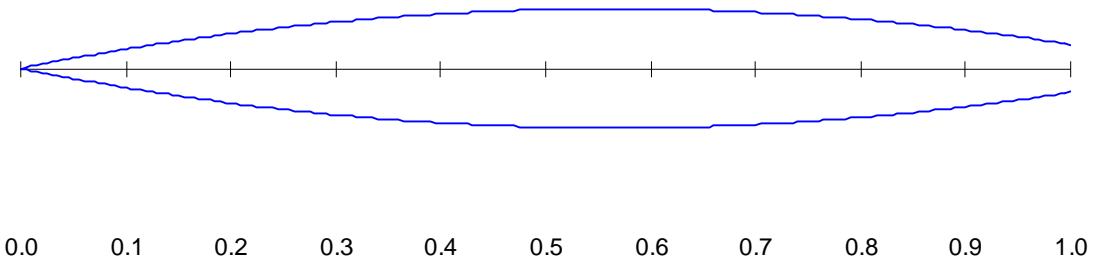
Figure 10   Parametric hull form - parabolic waterline.
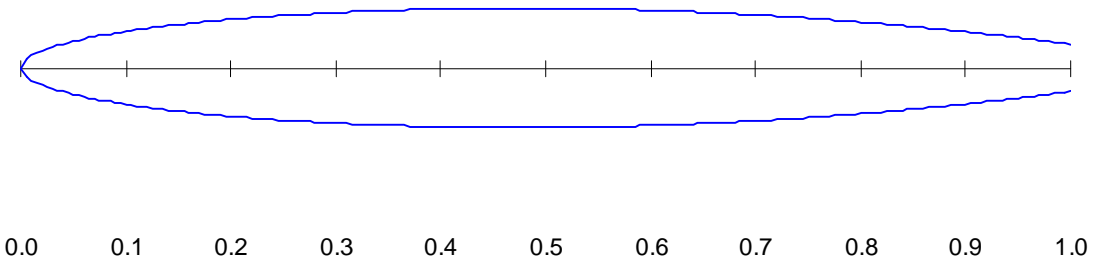
Figure 11   Parametric hull form - elliptical waterline with parabolic stern lines

The keel heights were described by a composite curve consisting of a vertical stem, elliptical forefoot, a baseline keel section and a parabolic stern section. The typical keel profile is shown in Figure 12. The top of the forefoot is also the top of the turn of the bilge. From this point up to the DWL, the hulls are wall sided.
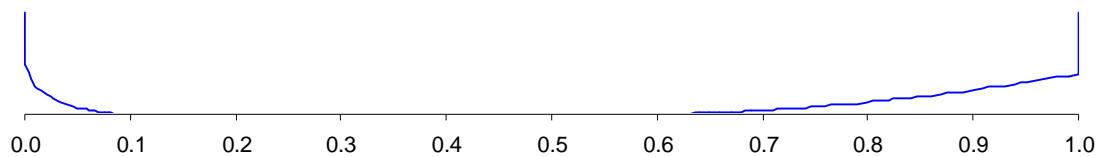
Figure 12   Parametric hull form - keel diagram, elliptical forefoot, parabolic stern

All transverse station sections in the hull (Figure 13) were developed by using key points from the keel and waterline formulas. From the keel up to the turn of the bilge, an ellipse was used. From this point up to the DWL, a vertical line was used.
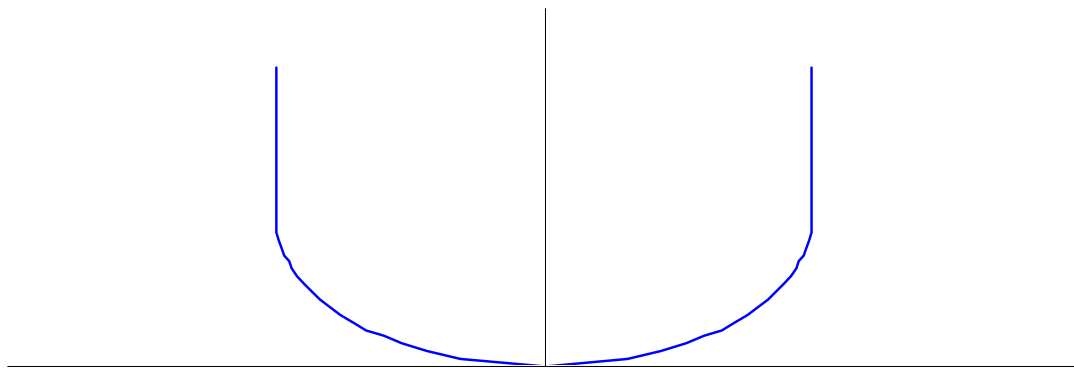
Figure 13   Parametric hull form - elliptical transverse section.

Once the equations for the parametric hull series were developed, the next step was to develop an automated process for creating the table of offsets that would be used by Michlet. This started out as a relatively small programming project that grew in scope.

The parametric hull generation program, known as HullGen, develops tables of offsets for Michlet based on the elementary parabolic and elliptical forms described above. It also has the ability to combine multiple (up to six) shapes or bodies in order to create features such as bulbous bows, skegs or SWATH struts. This allows for more complicated hull forms to be analyzed. A second program called MultiHyd was written to combine the hydrostatics outputs from HullGen so that complete hydrostatic files for multi-hulls could be calculated.

HullGen requires only 11 parameters to produce a hull. Table 2 shows an input file for creating a single hull for analysis with Michlet.[3] Up to six sets of parameters can be combined to create hulls with complex features such as bulbous bows or skegs.

---

[3] The parameters shown in Table 2 were used to create the main hull that was used for the hybrid hydrofoil Model B2.

Table 1   HullGen input parameters with Model B2 center hull data shown.

HullGen Hull Assembly Parameters	
1	Bodies in the Assembly
1	Body Number
70.00	Length (m)
5.00	Max beam (m)
0.50	Beam Aft (m)
4.00	Depth (m)
3.00	Bilge tang. (m)
2.00	Forefoot set back (m)
0.01	Keel hgt. aft (m)
4.00	Base line (m)
-	Fwd. perpend. (m)
P	W.L. type
O	Body type

2.2.2 - <u>Validation of Michlet</u>

By using Michlet to solve for the resistance of all of the hull form variations that would be tested, any errors that may be inherent in Michlet's results would be inconsequential because those same errors would equally affect all hulls analyzed. Although a number of validation tests of Michlet had been previously conducted, an additional test was conducted to determine the accuracy of Michlet in conjunction with HullGen.

A number of the Series 64 hull models resembled the types of hulls that HullGen can produce. Model 4787 was particularly reproducible by HullGen and was selected for the validation test. Figure 14 shows the lines of the HullGen model that was created for the test. The image portrays only the submerged portion of the model.
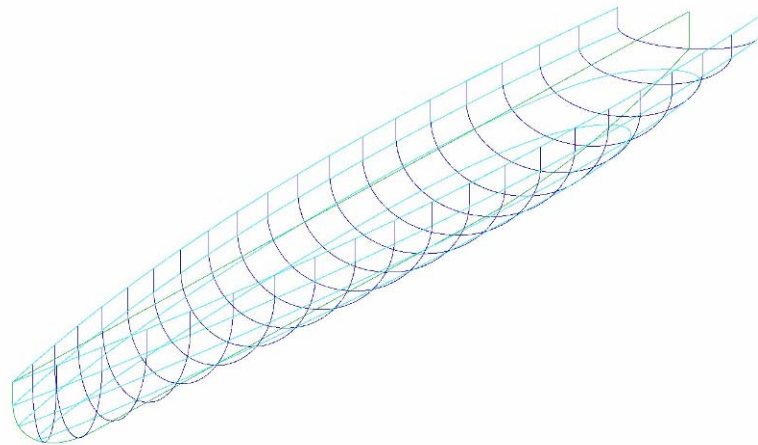
Figure 14   Lines image of the HullGen approximation of the Series 64 model 4787.

Michlet does not calculate lifting forces generated by the hull and it holds the hull model at a fixed attitude throughout the speed range of the resistance calculations. This introduces a degree of error by eliminating the effects of sinkage and trim. It compensates for this by allowing the user to specify sinkage and trim manually. The results shown in Figure 15 include the effects of experimentally recorded sinkage and trim values that were obtained from the model test. Without the sinkage and trim, Michlet under predicted the total resistance by approximately a 5% at the higher speeds. Taking this into consideration, there was still an excellent correlation between the model test and the Michlet calculations. The validation indicated that Michlet would be a suitable tool for making subsequent comparisons.
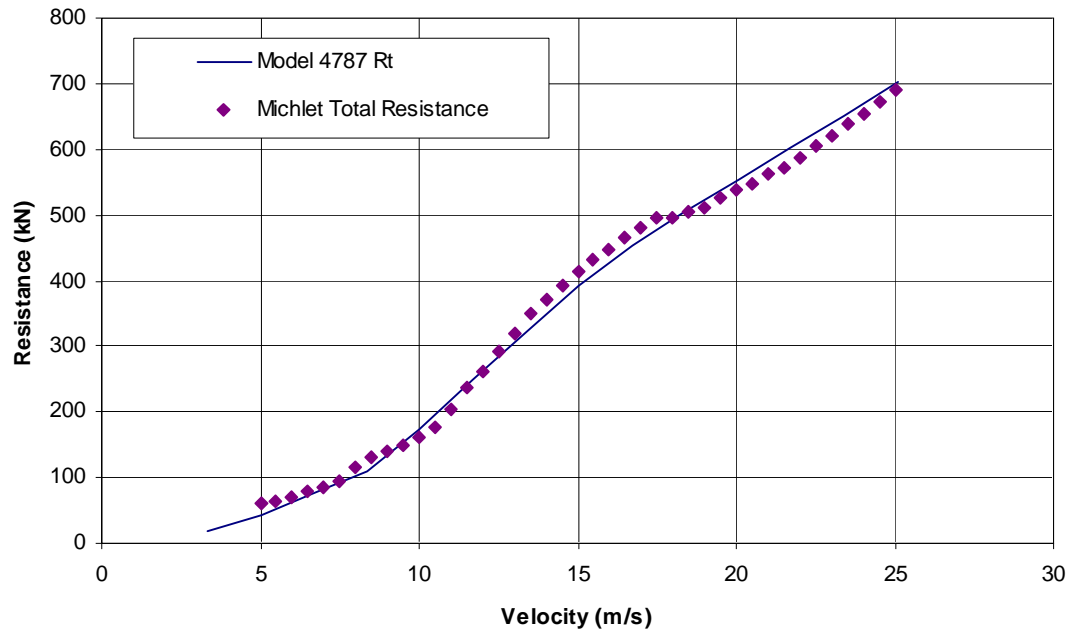
Figure 15   Model Series 64 model 4787 validation results for total resistance.

2.2.3 - Variation of Parameters

The primary objective of the parametric hull form studies was to determine the effects of varying length/beam and length/depth ratios on the total resistance. Later tests investigated the effects of the height of the bilge radius, forefoot setback and the height of the keel at the transom. The other geometric feature that was studied was the difference in performance between parabolic and elliptic design waterlines.

The results of initial tests were very sensitive to the length of the waterline and displacement. In order to normalize the tests, a fixed displaced volume of 1,000m^3 was imposed on all test hulls. This displacement was used throughout the project. It prevented unfair waterline advantages and placed a tangible value on the ship's potential to

earn money. Once beam and depth ratios were established for a particular model, length

was varied proportionally until the 1,000m^3 displacement was obtained.

Figure 16 shows the results of the parametric hull resistance studies. Each data

point represents the lift/drag ratio at a speed of 25 m/s (48.6 knots). In general, the higher

the length/beam ratio, the better the performance. L/D also increases as the length/draft

ratio increases. These results were not unexpected. Higher l/b ratios have been shown by

other researchers to exhibit the best performance.
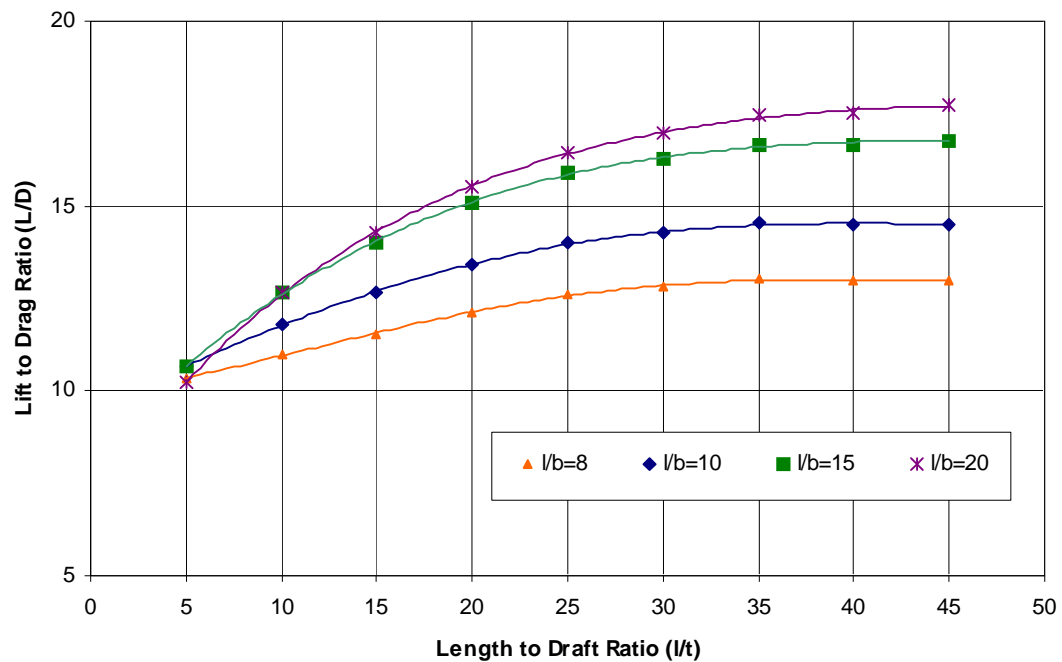
Figure 16   Effects of length/beam and length/draft ratio.

After completing the study of the effects of varying length/beam and length/draft

ratios, it was apparent that subsequent tests should have these parameters fixed. This

would prevent unfair advantages between the candidate hull forms that would be tested,

even though they would all displace 1,000m^3. The ratio selected was l/b = l/t = 10. These ratios would produce ships of reasonable proportions and are well within Newman's criteria for slenderness.

2.2.4 - Comparison of Hull Forms

The hull forms that were selected for this study included mono-hulls with both elliptic and parabolic design waterlines, catamarans, and Swaths. The cats were constructed from 500m^3 versions of the larger 1,000m^3 mono-hulls that were tested. The SWATH was unique, but the main submarine hull maintained the same l/b and l/t relationships of 10.0, as did the other test models. For the multi-hulls, a uniform length to lateral separation ratio (l/s) of 2.0 was used. This was done to normalize lateral separation effects between the different hulls. This ratio was considered a reasonable maximum for l/s. The dimensions of the test subjects are shown in Table 2. Results from the resistance testing are shown in Figure 17.
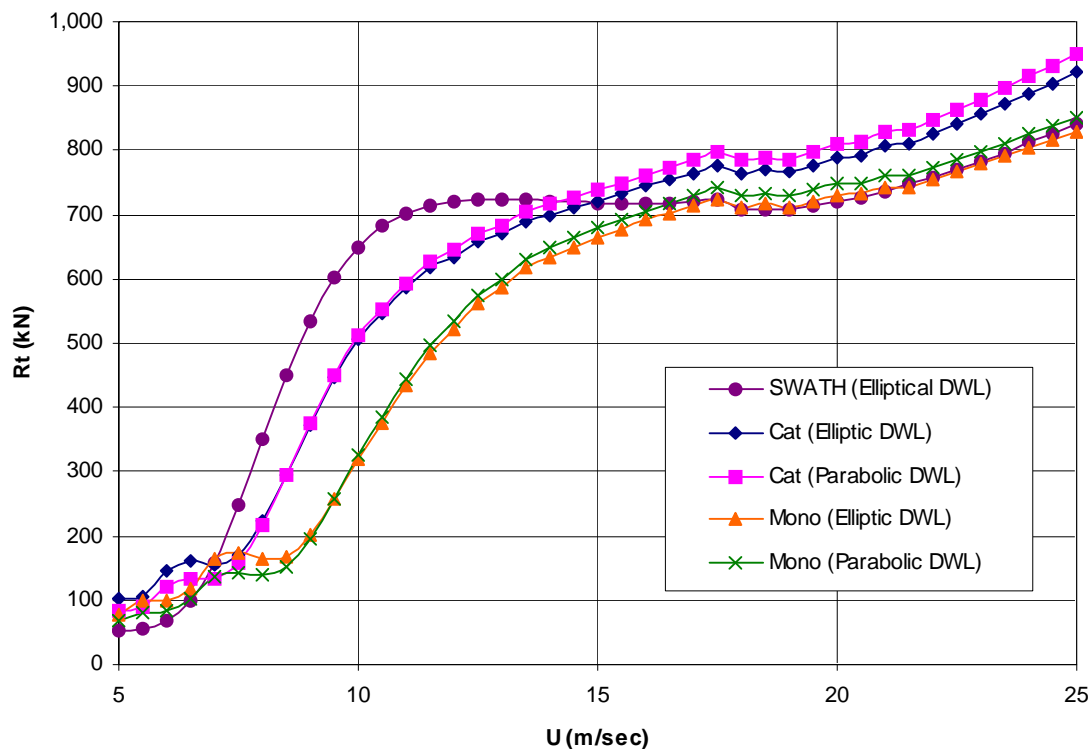
Figure 17   Resistance data for various hull forms of equal displacement.

Table 2   Dimensions of displacement hulls used in resistance calculations.

Model	Length	Beam	Draft	Surf Area	Lat Sep
SWATH	44.23	4.23	8.86	1,030	22.10
Mono (Ell. DWL)	54.34	5.43	5.43	650	-
Mono (Para. DWL)	56.13	5.61	5.61	688	-
Cat (Ell. DWL)	43.13	4.31	4.31	868	21.60
Cat (Para. DWL)	44.55	4.46	4.46	920	22.30

The SWATH (Figure 18) showed the lowest low speed resistance and the second lowest high-speed resistance. Unfortunately, the resistance increases dramatically between 7 and 11 m/s. This makes it an unlikely candidate for a vessel that will be

equipped with foils. If the estimates for L/D performance of a hybrid hydrofoil made in

Section 1 were accurate, reductions in resistance would not take effect until the speed of

the vessel exceeds a Froude number of approximately 0.7. This equates to velocities be-

tween 14 and 16 m/s for vessels of this length range. By the time the SWATH reaches

this velocity, it is encountering over 80% of the total resistance that it will develop at top

speed (25m/s). This means that a propulsion system sized for the SWATH would have to

develop significantly higher thrust levels at take-off speed than other craft with the same

top speed resistance.
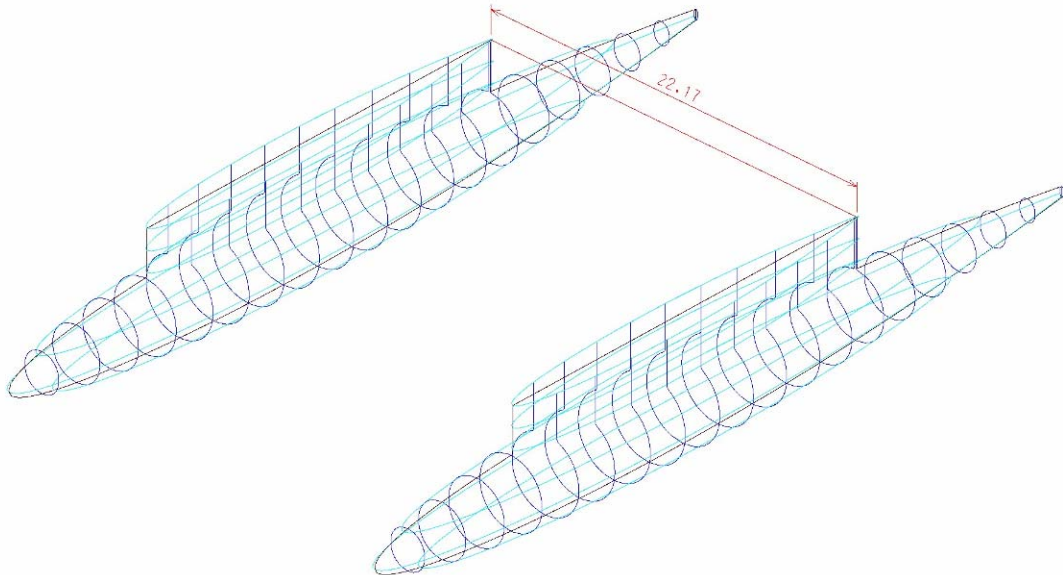
Figure 18   Lines image of a 44.2m SWATH.

The SWATH form introduces other problems that impede the development of a

hybrid. Conceptually, the SWATH form cannot be hybridized to a great extent because a

large portion of its buoyancy is located close to the baseline. There is no practical way to reduce the buoyant lift of a SWATH by reducing its draft without putting it into a condition that would cause serious problems with resistance and stability. Additionally, according to Lee and Curphey [8], SWATHs become longitudinally unstable at higher speeds due to the presence of the destabilizing moments that are generated by dynamic pressure differentials along the hulls. Michlet is not capable of predicting the effects of these phenomena and the resulting resistance calculations were subsequently considered to be optimistic.

The catamarans tested in this exercise faired better than the SWATH, but they too developed significant resistance levels by the time they reached the 14-16m/s speed range. The data also shows that although the cats outperformed the SWATH in the mid-range speeds, they were the poorest performers at all other speeds. An image showing the lines of the catamaran with parabolic waterlines that was tested is shown in Figure 19.
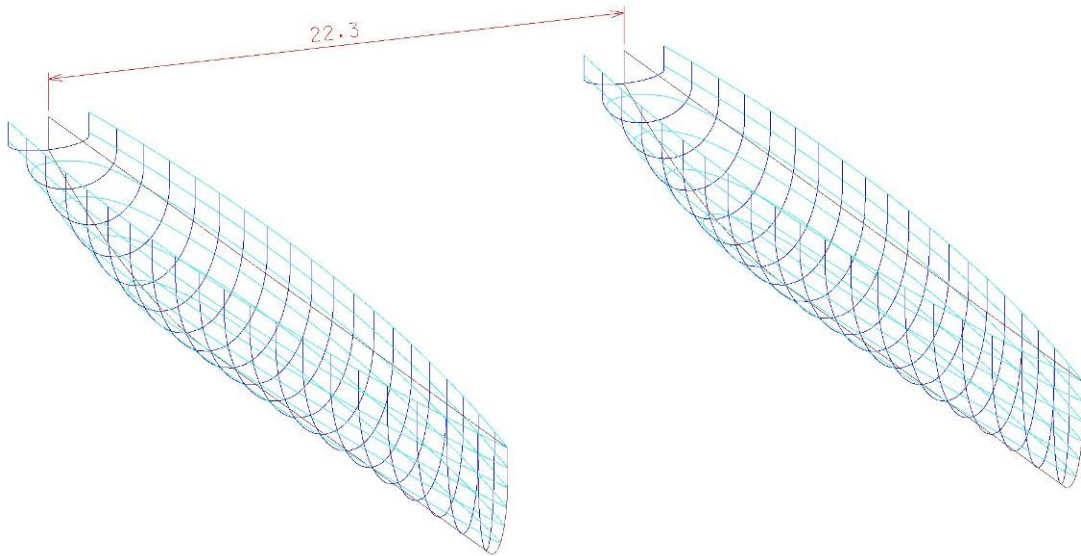
Figure 19   Lines image of a 44.6m catamaran with parabolic waterlines.

The models with the best overall performance were the slender mono-hulls. They exhibited the least resistance in the speed range where the "hump" is expected to develop. Figure 20 shows an image of the lines for the mono-hull with an elliptic DWL. This model showed higher resistance than the mono-hull with a parabolic DWL at speeds less than 9m/s, but lower resistance at the higher speeds.
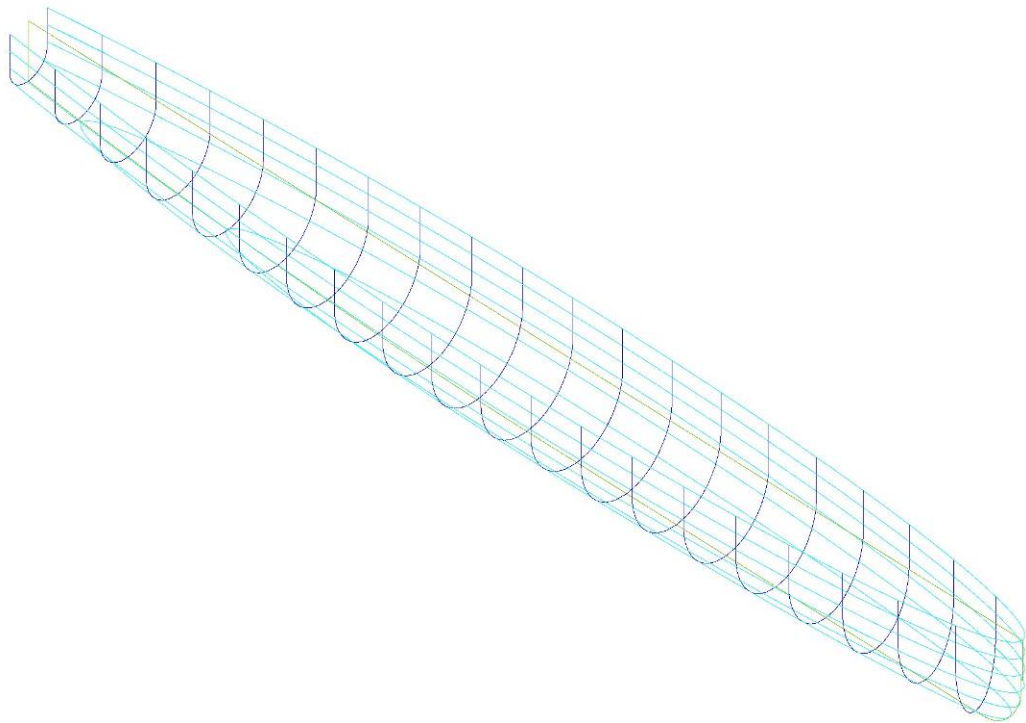
Figure 20   Lines image of a 54.3m mono-hull with an elliptic DWL.

Results of this series of tests lead to the conclusion that a final test should be conducted between the best of this group. The test craft would consist of a mono-hull with a parabolic waterline and a semi-SWATH vessel known as HYSWAS. An image of the HYSWAS that was tested in this last comparison is shown in Figure 21. It consists of a single SWATH hull attached via a strut to a mono-hull. The HYSWAS form eliminates the geometric problems associated with decreasing the SWATH's draft as stated earlier. It does not eliminate the longitudinal stability problems and compounds the problem by introducing roll and yaw instabilities as well.
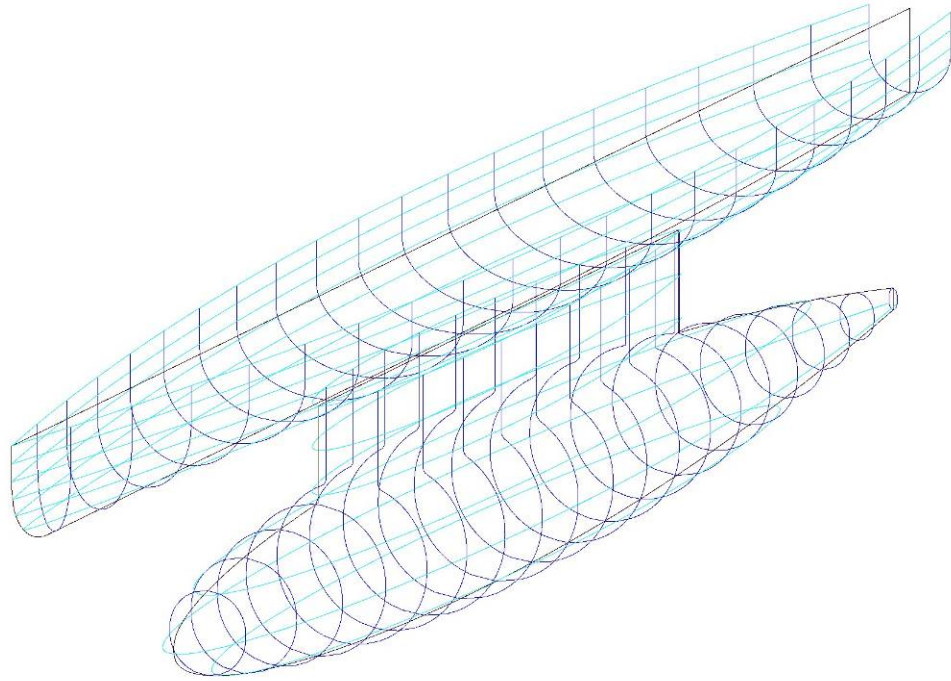
Figure 21   Lines image of a 55.2m HYSWAS.

Since the earlier work accomplished in this project indicated that less than 50% of

the total lift at top speed would be generated by buoyancy, the finalists were tested at

1,000m^3 and 500m^3 displacements. This was done to investigate the differences in the

drag contributions of each hull in the reduced displacement condition. The results of the

resistance analysis are shown in Figure 22. The winner of this contest, is not clear. The

HYSWAS has higher mid-range resistance but lower bottom and top end resistance. It

would be the winner if top end performance was the only issue, but it is not. Dynamic

stability problems must also be considered. Conquering these would involve the devel-

opment of a sophisticated flight control system, which is not in keeping with practical

objectives of the project. Ultimately, the HYSWAS form was abandoned in favor of the

slender mono-hull.[4] The slender mono-hull is not without it's stability problems however

and a solution for pitch and roll instabilities would have to be developed before a slender

mono-hull design would "fly".
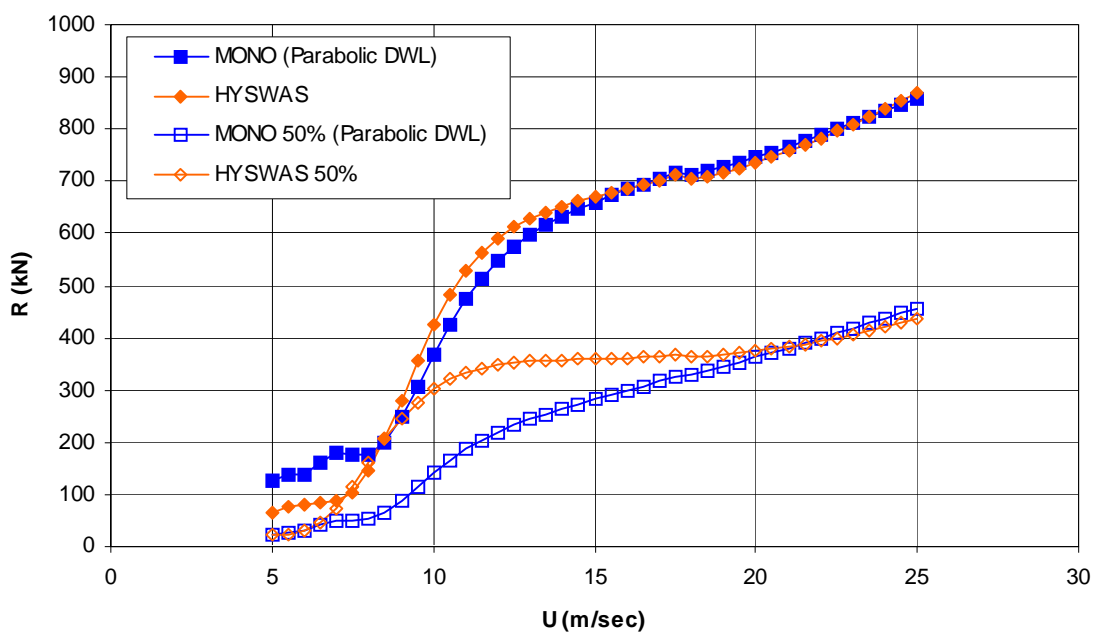
Figure 22   Comparison of mono-hull and HYSWAS resistances.

---

[4] As the project progressed, the decision to make the hybrid craft a full flier was made. This would not

have been a viable alternative for the HYSWAS form.

3 - HYBRID HYDROFOIL PERFORMANCE ANALYSIS

The prediction of the performance of a hybrid hull form requires specialized soft-ware that is capable of calculating the total resistance of the vessel. Michlet alone can not compute the resistance of this type of craft and new software had to be developed for the task. That software, known as Hy2Perf, is designed to solve the coupled equations of surge, heave and pitch for a ship in the time domain.

3.1 - Time Domain Solution of Coupled Equations of Motion

The theory of operation employed by Hy2Perf is relatively basic. The calculation is conducted in the time domain. This means that each calculation run consists of a fixed number of time steps. In most cases the vessel is accelerated from rest at time T=zero. The program then calculates all of the forces and moments exerted on and by the vessel. These forces and moments are summed and then resolved into accelerations using the coupled equations of motion for surge, heave and pitch [1], shown in Equations 16 – 18. Once the accelerations are computed, they are used to compute velocities and displace-ments at the end of the time step. This basic process is followed during each time step.

Surge:
$$\sum F_1 = m\left(\ddot{\eta}_1 + \bar{Z}_C \, \ddot{\eta}_5 \right) \tag{16}$$

Heave:
$$\sum F_3 = m\left(\ddot{\eta}_3 - \bar{X}_C \, \ddot{\eta}_5 \right) \tag{17}$$

Pitch:
$$\sum F_5 = m\left(\bar{Z}_C \, \ddot{\eta}_1 - \bar{X}_C \, \ddot{\eta}_3 \right) + I_{55} \, \ddot{\eta}_5 \tag{18}$$

Where: F_1 = Forces in the axial (fore/aft) direction

F_3 = Forces in the vertical direction

F_5 = Moments about the transverse axis

I_{55} = Moment of inertia about the pitch axis

m = Mass of the vessel

Zc = Vertical center of gravity

Xc = Longitudinal center of gravity

$\ddot{\eta}_i$ = Accelerations, surge: i=1, heave: i=3, pitch: i=5

The surge, heave and pitch accelerations cannot be determined directly from Equations 16 – 18. Therefore, the equations were rearranged to provide direct solutions. Since the pitch acceleration equation is the coupling agent between heave and surge, it was resolved first. It was then substituted into the acceleration equations for heave and surge to obtain those accelerations. The solution is shown in equations 19 – 21.

Pitch:
$$\ddot{\eta}_5 = \frac{F_5 - \bar{Z}_C F_1 + \bar{X}_C F_3}{-m\bar{X}_C{}^2 - m\bar{Z}_C{}^2 + I_{55}} \qquad (19)$$

Heave:
$$\ddot{\eta}_3 = \frac{F_3}{m} + \bar{X}_C \ddot{\eta}_5 \qquad (20)$$

Surge:
$$\ddot{\eta}_1 = \frac{F_1}{m} - \bar{Z}_C \ddot{\eta}_5 \qquad (21)$$

The program treats accelerations computed during each time step as constants. At the beginning of each time step, all forces and moments are computed, summed and then

used to compute the pitch acceleration. The pitch acceleration and the sum of the forces in surge and heave are then used to compute the surge and heave accelerations respectively. The three accelerations are then used to solve for the velocities and displacements for the next time step. These values are then used to compute the forces and moments that will be developed at the initiation of the next time step. The forces are computed by a variety of methods. A detailed explanation of the method of calculation for each force is contained in the following sections.

3.2 - Gravity Forces

The gravity forces are generated by two different means. These are the masses of the components comprising the vessel and its cargo, and the buoyant force generated by the hull or hulls. The data concerning the mass and location of parts of the vessel, its cargo and liquids, such as fuel and water, are contained in a parameter file. The file also contains information concerning the hull offsets, resistance tables and key variables governing the performance prediction.

The mass of the vessel, center of gravity and mass moment of inertia are computed during each time step. This is necessary because the entire craft is continuously changing location with respect to the waterplane, subsequently altering the moments exerted by the masses.

The hydrostatic or buoyant force is calculated from hull offsets during each time step. The offsets and the orientation of the hulls with respect to the vessel's baseline, centerline and forward perpendicular are all contained within the parameter file. These values are adjusted with respect to the waterplane location after each time step and a new

displacement and center of buoyancy is computed from the table of offsets. The water-line is presumed to be linear, ignoring the second order effects of waves.

3.3 - Hydrodynamic Forces

The hydrodynamic forces consist of all the forces that are functions of the speed of the vessel. These consist of the thrust of the propulsor, the resistance of the hulls, and the lift and drag generated by the foils. The methods used to determine these forces are discussed in the following sections.

3.3.1 - Resistance and propulsion

The thrust force used by Hy2Perf is generated by a notional propulsor. Since the actual characteristics of the propulsor were not known at the beginning of this project, a theoretical propulsor was used. This propulsor was assumed to produce thrust as a function of the vessel's velocity. A linear function was used to increase thrust to a peak value and then a parabolic function was used to decrease the thrust as the velocity increased beyond the peak thrust point. Figure 23 shows a plot of thrust versus velocity for this type of propulsor. The notional thrust curve is meant to simulate the steady increase in thrust that would be experienced by increasing power to the maximum available. This is followed by the drop in thrust that is typical for most propulsors operating at a constant power, as speed increases.
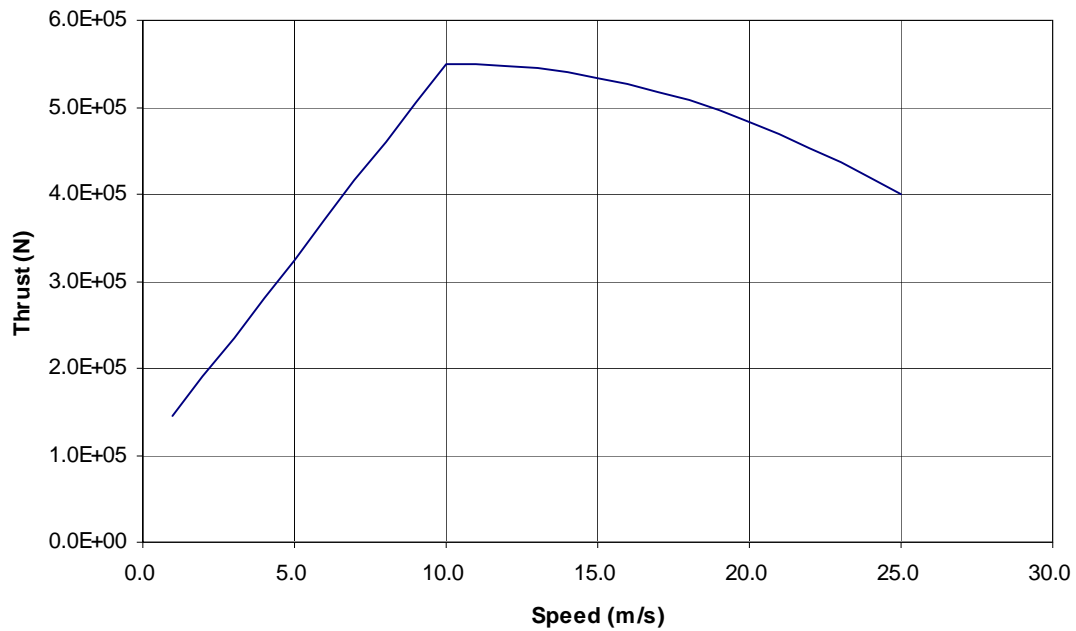
Figure 23   Typical thrust curve used by Hy2Perf.

This approach to simulating the performance of the unknown propulsor is based on the philosophy that the resulting thrust curve would serve as a design parameter for selecting the actual propulsor that would eventually be used. Once a propulsor that meets the general requirements is selected, its actual performance curve could be substituted for the notional thrust curve and the performance prediction could be refined.

The resistance of the hulls was calculated by Michlet prior to beginning the hybrid calculations with Hy2Perf. This was a relatively time consuming process because it involved multiple calculations. Since the hybrid hull gets lifted out of the water as speed increases, the attitude and elevation of the hull for any given time step were impossible to predict in advance. This subsequently made the calculation of the resistance for a particular speed by Michlet, an impossibility.

In order to circumvent the problem, a table of resistances was generated for the vessel. A matrix was developed to cover all displaced volumes ranging from full load to zero. For each displaced volume, resistances were computed for a range pitch angles. The resistance matrix consisted of 24 individual resistance tables, each containing resistance values computed for speeds ranging from 5 m/s up to 25 m/s. Displaced volumes of 100%, 75%, 50%, 25%, 12.5% and 0, in combination with pitch angles of −1, 0, 1 and 2 degrees were used to build the matrix. This range of factors covered all of the possible extremes for pitch, heave and velocity that the vessel's hulls might encounter.[5] Once the table of resistances was computed by Michlet, the resistance for any given pitch, heave and velocity was determined by interpolation.

3.3.2 - Hydrofoil forces

The lift and viscous drag forces generated by the hydrofoils were calculated using Bernoulli's equation as shown in Equation 22. The lift coefficient used in this formula was treated as a design parameter for later use in developing the foils. The program calculated the lift coefficient of each foil based on Equations 22 - 24. The angle of attack included any adjustments made by the program for control purposes plus the changes in pitch of the hull.

$$L = \frac{\rho}{2} U^2 S C_{LW} \qquad (22)$$

---

[5] In general, Hy2Perf holds pitch attitudes to nearly zero and the wide range of the pitch variable could have been narrowed considerably.

Where L = Total lifting force

U = Velocity

S = Foil plan form area

C_{LW} = Lift coefficient, 3D wing (foil).

$$C_L = 2\pi(\alpha - \alpha_i) + C_{Ld} \qquad (23)$$

Where C_L = 2D lift coefficient of the foil

C_{Ld} = 2D design lift coefficient at zero angle of attack

α = Foil angle of attack (radians)

α_i = Foil installed angle of attack (radians).

$$C_{LW} = \frac{C_L}{\left(1 + \dfrac{2}{AR}\right)} \qquad (24)$$

Where C_{LW} = 3D lift coefficient of the foil

C_L = 2D lift coefficient from Equation 23

AR = The foil's aspect ratio, span^2 divided by plan form area.

The slope of the lift coefficient curve used in Equation 23 was 2π. This slope is a function of the foil's proximity to the free surface and the value 2π is valid only if the foil is deeply submerged. In practical terms, this equates to a minimum of five chord lengths from the surface. Numerous studies and theoretical works have been developed concerning the changes to the lift curve slope as a lifting surface approaches the free surface. The lift curve slope decreases until the foil broaches the surface, at which time it becomes

π. According to studies conducted at the Langley Aeronautical Laboratory in the 1950's by Wadlin and Christopher [12][13], the reduction in lift becomes significant when the ratio of the depth of submergence to foil's chord length reaches values of 2.5 or less. In the initial versions of Hy2Perf, this lift reduction was simulated by an elementary, parabolic equation based on the depth to chord ratio. This was later changed to a more accurate polynomial that was based on results from the lifting line program described in Section 5.

The total drag coefficient is the sum of twice the friction coefficient obtained from Equation 5, plus the induced drag coefficient for the wing obtained from Equation 25. Doubling the friction coefficient allows the same plan form area to be used while accounting for the viscous friction on both the upper and lower surfaces of the foil. Since the induced drag is a function of the lift coefficient of the wing, it too is affected by the proximity of the wing to the surface. These empirical adjustments were refined after analysis by the vortex lifting line program was completed.

$$C_{Di} = \frac{C_{LW}^2}{\pi AR} \qquad (25)$$

3.4 - Aerodynamic Forces

Aerodynamic forces were not considered in this study. Although placeholders that store the vessel's topside surface area distributions and drag coefficients were written into the code, aerodynamic drag calculations were not implemented. There were three primary reasons for not implementing this calculation. First, it was presumed that for comparative purposes, the various hulls considered would all have equivalent topside

configurations and aerodynamic drag. The second reason for not including aerodynamic drag in the study was that this drag does not contribute significantly, as compared to the hydrodynamic drag, until speeds exceed 50 knots. Since 25m/s (approximately 49 knots) was the top speed used in this study, aerodynamic drag was not considered. The final reason for not including aerodynamic drag in the study was to conserve time.

3.5 - Hy2Perf, Hybrid Hydrofoil Performance Computer Program

Hy2Perf operates as a menu-driven DOS application. As the program loads, it prompts the user for the name of a parameter file. This file contains all of the data required to describe the hybrid vessel's geometry, its loads, resistance characteristics and thrust curve. When the parameter files have loaded, the user can change various settings and run time variables that control the duration of the calculation, number of time steps to be executed and the initial conditions of the hull. It also allows the user to launch subsequent performance runs from the state that the previous run ended, allowing for extended calculations if the desired state is not achieved by the end of a particular number of time steps.

The calculation is not strictly a matter of grinding through 10,000 time steps and producing an answer. The program must compensate for the changes in attitude of the hull as it accelerates. This is done by adjusting a set of control surfaces. The program assumes that the first two lifting surfaces read from the parameter file are trim planes. Hy2Perf determines whether the planes are bow or stern planes, depending on their coordinates. This is important because the correct sign must be applied to the angle of attack adjustments. The parameter file also contains a pitch range setting for Hy2Perf to main-

tain, as well as maximum angles of attack and rates of change for the planes. On start-up, the foils will generally be adjusted to their maximum setting, where they remain until the speed of the vessel increases enough for the planes to have an affect on the pitch. Then the bow plane algorithm adjusts the bow plane angle of attack until the hybrid ship is within the pitch limitations set in the parameter file.

All of the destabilizing forces developed while Hy2Perf is executing are strictly the result of changes in the force balance between time steps. Hy2Perf calculates the lift generated by lifting surfaces and does not calculate unsteady forces that may be acting on the hull surfaces.

In addition to pitch control, the user can set a target maximum speed for the vessel. Hy2Perf will allow the craft to accelerate based on the computed thrust until it reaches the maximum speed input by the user. Once this speed is reached, the thrust curve is adjusted until a steady state is achieved for the desired speed or until the time steps for the calculation have been used up. If a steady state is not reached before this happens, the calculation can be continued for another fixed number of time steps as determined by the user.

The ultimate height that the hulls can achieve is determined by the location of the foils below the bottom of the hull and the top speed of the vessel. There is no height control algorithm in this version of the program. Height is controlled strictly by the top speed and the characteristics of the foils. The program is not sensitive to the free surface proximity and will not compute the point at which ventilation is likely to occur. It will accept foil arrangements with dihedral angles and allow them to penetrate the surface.

To do this however, it mathematically deletes the portion of the foil that has broached and is in the immediate proximity of the surface.

There are two triggers built into Hy2Perf that will stop execution of the program. The first trigger is based on excessive pitch angles and rates of change in pitch. Effectively, this trigger detects a "plow-in" event and stops the program before it crashes, allowing the user to save the data computed up to the point of the event. This feature was very useful in troubleshooting various foil configurations that were tried. Several of these configurations were unstable.

The second trigger that will stop execution of the program is the detection of cavitation on a foil. The foils used in this study are considered to be of a fully wetted, NACA 66mod design. If cavitation breaks out on this type of foil, lift can be expected to break down rapidly and the program is not designed to compute the physical effects of this type of phenomenon. To account for the presence of cavitation and to avoid its outbreak, the criterion developed by Brocket [3] was used. Equation 27 was used to determine the optimum foil thickness throughout the speed regime. Hy2Perf continuously checks to ensure that the input thickness does not exceed the optimum. This formula is valid for a NACA 66mod, 2D foil section with a 0.8 mean line. It uses the fluid velocity, lift coefficient and cavitation number to determine the optimum thickness for avoiding cavitation. The cavitation number was calculated using Equation 26 and the Brocket optimum thickness is calculated by Equation 27.

$$\sigma = \frac{P_{Hyd} + P_{Atm} - P_{Vap}}{\frac{\rho}{2} U^2} \tag{26}$$

Where: σ = Cavitation number

                P_{Hyd} = Hydrostatic pressure given by $\rho g h$

                P_{Atm} = Atmospheric pressure

                P_{Vap} = Vapor pressure of water

$$t_B = -3.008C + (0.334 - 0.425C)\sigma \tag{27}$$

Where: t_B = Brocket optimum foil thickness ratio (max thickness/chord)

                C = Foil camber (= $0.0679C_{LW}$).

During each time step execution, the Brocket optimum thickness is calculated for each foil. If the optimum thickness falls below the design thickness for any of the foils, a warning is given to the user and execution of the program is halted. This prohibits the calculation of performance that is not physically achievable.

A typical performance evaluation consists of two steps. The first is a zero thrust stabilization run. When the data is input, all coordinates for the hulls, cargo, foils, weights, other components are referenced from either the design water plane or the main hull's baseline. During the stabilization run, the vessel is allowed to assume a natural static equilibrium condition. The second step is to conduct a resistance calculation, during which time the craft is accelerated from rest up to the maximum speed input by the user or until the thrust and resistance equalize. Calculation continues until the desired number of time steps are executed.

Hy2Perf holds the data computed for each time step in memory during an execution and presents the user with data "snapshots" throughout the process. When the calculation is complete, the user can save all or a percentage of the data developed during

the run. A typical calculation will last up to 10,000 time steps of 0.01 seconds each. This amount of data is required for numerical stability, but is not required for analysis after the calculation is complete. The data can be reduced by saving intermediate time step results and discarding the rest. A reduction factor of 90% provides satisfactory plots of the results. The output data includes the following entries: elapsed time, forward and aft keel drafts, angle of attack of the trim planes, propulsor thrust, total resistance, and the displacement, velocity and acceleration value for each of the three principle axes (surge, heave and pitch).

4 - FOIL PERFORMANCE ANALYSIS

The hybrid hydrofoil performance program Hy2Perf was developed as a design tool to assist in evaluating the factors required to produce an improvement in conventional displacement hull performance. As such, the program relied heavily on the work and formulations of previous researchers. This work enabled the combination of hull resistance characteristics with established air and hydrofoil formulas to produce an overall performance prediction for a hybrid vessel. In an effort to refine the performance prediction of Hy2Perf, a final program that evaluated the performance of hydrofoils operating near the free surface was developed. This program was called LiftLine.

4.1 - LiftLine, Vortex Lifting Line Computer Program

LiftLine is a vortex lifting line program that is capable of calculating the three dimensional lift and drag coefficients for arbitrary foil geometries. The code was based on the Prandtl lifting-line model as implemented by Katz and Plotkin [6]. This model places a bound linear vortex element system on the lifting surface and trails vortex line elements aft and into the wake of the foil. The strength of the vortex elements is presumed to be constant and is resolved through the solution of a linear set of algebraic equations. The velocities induced by each bound vortex element and its trailing wake elements are computed according to Equation 28. Figure 24 provides a diagram of a vortex line element and indicates the nomenclature and directions of the variables identified

in Equation 28. The velocity vector $\hat{q}_{1,2}$, is induced at point P by the circulation of the

vortex element extending from point 1 to point 2.

$$\hat{q}_{1,2} = \frac{\Gamma}{4\pi} \frac{\hat{r}_1 \times \hat{r}_2}{\left|\hat{r}_1 \times \hat{r}_2\right|^2} \hat{r}_0 \bullet \left(\frac{\hat{r}_1}{r_1} - \frac{\hat{r}_2}{r_2} \right) \tag{28}$$

Where Γ = Gammah, circulation

$\hat{r}_i$ = Unit vector

r_i = Radius
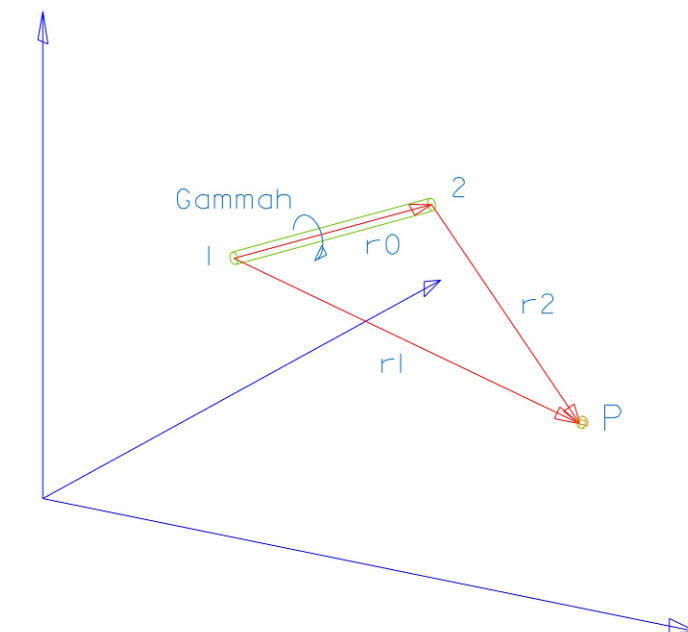
Figure 24   Vortex line element diagram.

LiftLine uses a distribution of vortex line elements similar to the one shown in

Figure 24 to obtain the induced velocities over the lifting surface. Figure 25 shows a typ-

ical hydrofoil in 3D space. The foil is divided into panels, each of which contains a

vortex line system consisting of a bound span wise element and four chord wise elements. Eight panels are shown in Figure 25, but the foil models that were analyzed in the next section usually were divided into 250 panels. A typical horseshoe vortex line system is shown on panel six. The chord wise wake elements, which begin one quarter chord length aft of the trailing edge, extend 20 chord lengths aft of the foil parallel to the onset flow, which is indicated as "Qinf." The bound span wise element and the two trailing chord wise elements are located in the plane of the wing. The bound span wise element is located one quarter chord aft of the leading edge. The collocation point (indicated by the "x") is located in the center of the panel in the span wise direction and one quarter chord length forward of the trailing edge of the wing.
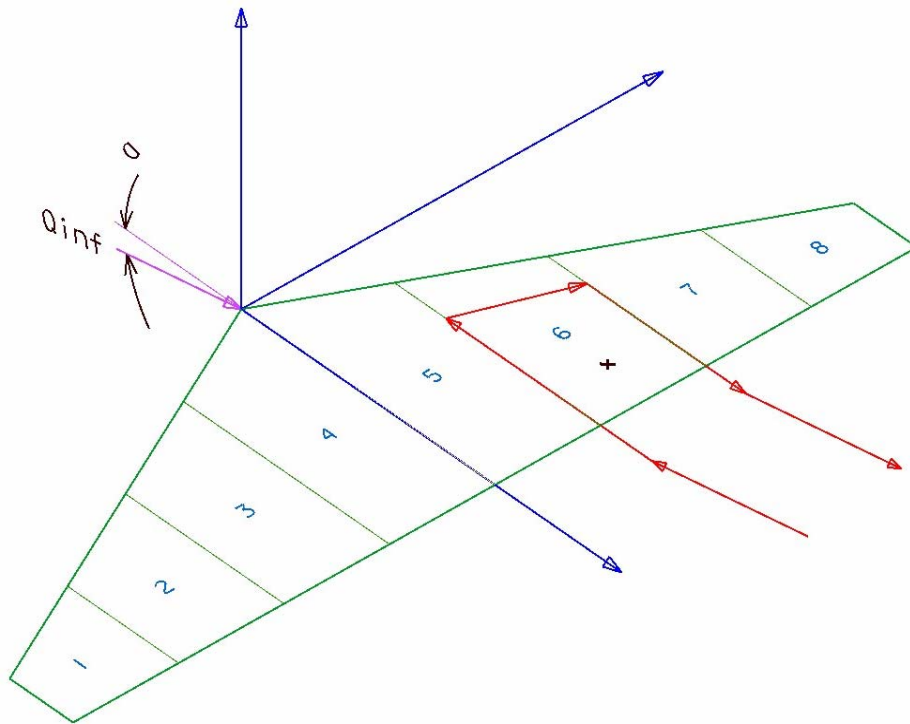
Figure 25   Panel and linear vortex element (horseshoe) arrangement on a 3D wing.

LiftLine calculates the induced velocities at each of the collocation points and integrates the flow to compute the lift, and induced drag for the wing. It then computes the lift, induced drag and viscous drag coefficients. It is a no-frills program that requires explicit geometry input in tabular format. The program will only calculate flat plan forms, but the plan form shape is unrestricted. In order to calculate the effects of the free surface, the program was written to accept multiple foil inputs and it calculates the combined influence of all of the foils simultaneously. This was done so that an image foil could be modeled above the main foil, simulating the free surface effect. The capability of processing multiple foils in the 3D space also provided the ability to calculate the effects of the foils upon each other as well as the effects created by the free surface.

Due to time constraints, the effects of the free surface on the main foil were primarily studied. The wake model used in LiftLine trails the vortex wake elements away from the foil at the angle of attack, parallel to the free stream. In order to properly model the wake effects on trailing foils, a more rigorous treatment of the wake modeling code and possibly a wake stepping routine would be required. In addition, the angle of attack of the foils was not always the same for the main foil and trim planes. The first implementation of LiftLine applied the same angle of attack to all foils in the 3D space.

Input for LiftLine consists of basic foil geometry. The leading and trailing edge coordinates of each foil to be calculated are read in from a single data file. The file also includes the water density and kinematic viscosity. Once the foil geometry is read into the program, the user is prompted for an angle of attack and velocity of the foil. The re-

sults are then displayed on the screen and saved to a file. Typical output for a single foil is shown in Table 3.

Table 3   Sample output data from LiftLine.

```
Output from SimpleLL
Modified_Delta_Planar_Surface
AoA              3
Velocity        20

Foil 1 Origin   2.00    0.00    0.00

Foil Data
Foil            Span  Chord    AR    Area     Cl     Cdi     Cdv    L/D
1               25.00   3.00   8.33   75.00   0.25  0.0031  0.0046  32.25
```

4.2 - Geometry and Free Surface Studies

The primary purpose for developing LiftLine was to verify the formulas used to modify the lift curve slope used by Hy2Perf when calculating the lift coefficients for foils near the free surface. The secondary purpose was to test the input data used by Hy2Perf and determine if foils matching the Hy2Perf input specifications could be developed from simple geometries.

A series of tests was conducted on various foil configurations in an attempt to simulate the desired performance of the elliptical formulas used in Hy2Perf. The geometries tested included elliptical, rectangular, tapered and modified delta wings. The modified delta consisted of a swept leading edge and a straight trailing edge that was held perpendicular to the centerline. The elliptical foil was used as the benchmark for testing the program and for evaluating the more elementary plan form geometries.

The plan form geometry study concluded that a modified delta wing could produce lift to drag ratios that equaled the performance of the elliptical foils. Figure 26 shows a plot of the lift to drag ratios calculated for modified delta foils operating at a depth to chord ratio of 1.0. All of the foils had the same aspect ratio, plan form area and angle of attack. The figure shows that a taper ratio of 20% provides the optimum lift to drag ratio for this type of foil. In that configuration, the modified delta is capable of a L/D of approximately 25.3. This compares favorably with the elliptical foil of equivalent aspect ratio and plan form area, which achieved a L/D of 25.1. This study showed that an elementary geometry could be used to produce the elliptical load distribution performance. A diagram of the modified delta plan form is shown in Figure 25.
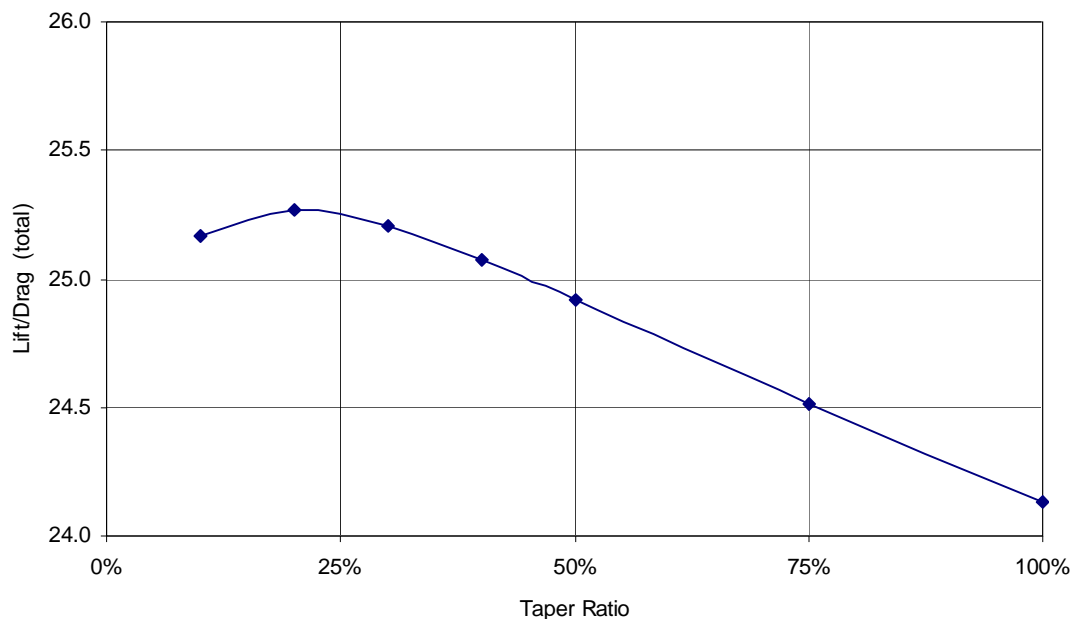
Figure 26   Effects of taper ratio on the lift/drag ratio of modified delta wings.

The second part of the study involved determining the effects of the free surface on the performance of the foil. To do this, duplicate foils arranged in a bi-plane configuration were analyzed. The foils were tested at distances ranging from four chords down to one quarter of a chord. This simulated submergences ranging from two chords down to one eighth of a chord depth. Figure 27 shows the results of the study. The elliptical foil maintained marginally super performance throughout the range of depths tested. The modified delta tested in this series used a 25% taper ratio and produced slightly lower performance than the elliptical plan form. The tapered and rectangular plans did not perform as well as either of the previous foils.
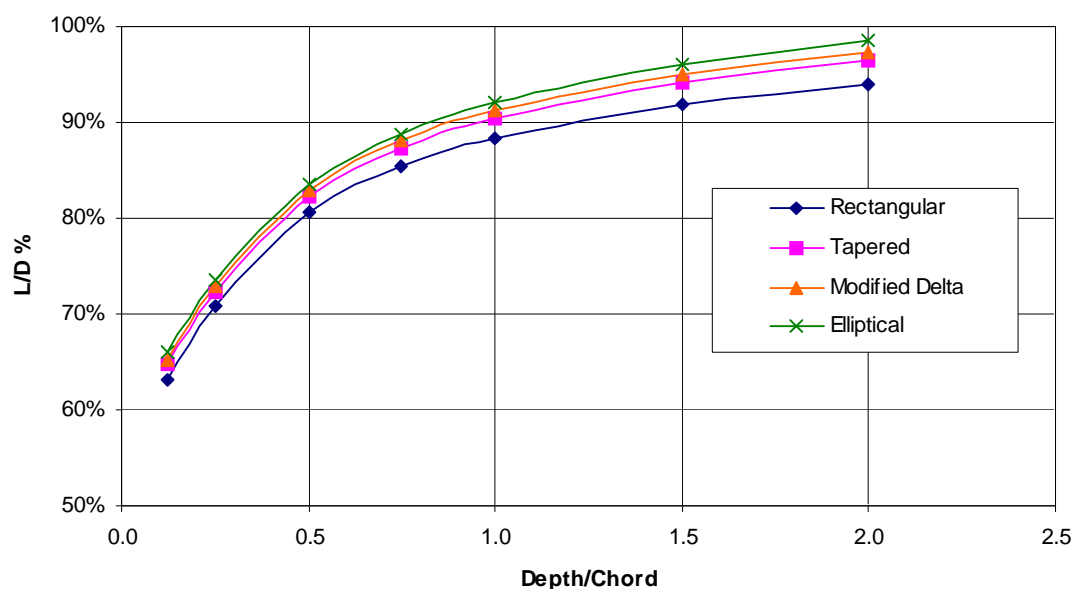
Figure 27   The effects of free surface proximity on the lift/drag ratio of wings.

The data shown in Figure 27 includes viscous friction, which is independent of the depth of submergence. In order to obtain factors for the induced drag and lift coeffi-

cient, these coefficients were plotted and polynomials were fitted to each set of data. Figures 28 and 29 show the changes in the lift coefficient and induced drag coefficient for each of the plan forms at various depth to chord ratios.

The foils used in the design of the hybrid craft are always within two chord depths of the surface. At that depth, the maximum lift curve slope is approximately 95% of the infinite depth slope or 1.9π. The induced drag coefficient however exceeded the infinite depth value by up to 10% in this depth range. From this data polynomials tailored to modify the lift curve slope and induced drag were obtained. These formulas are provided in Equations 29 and 30.
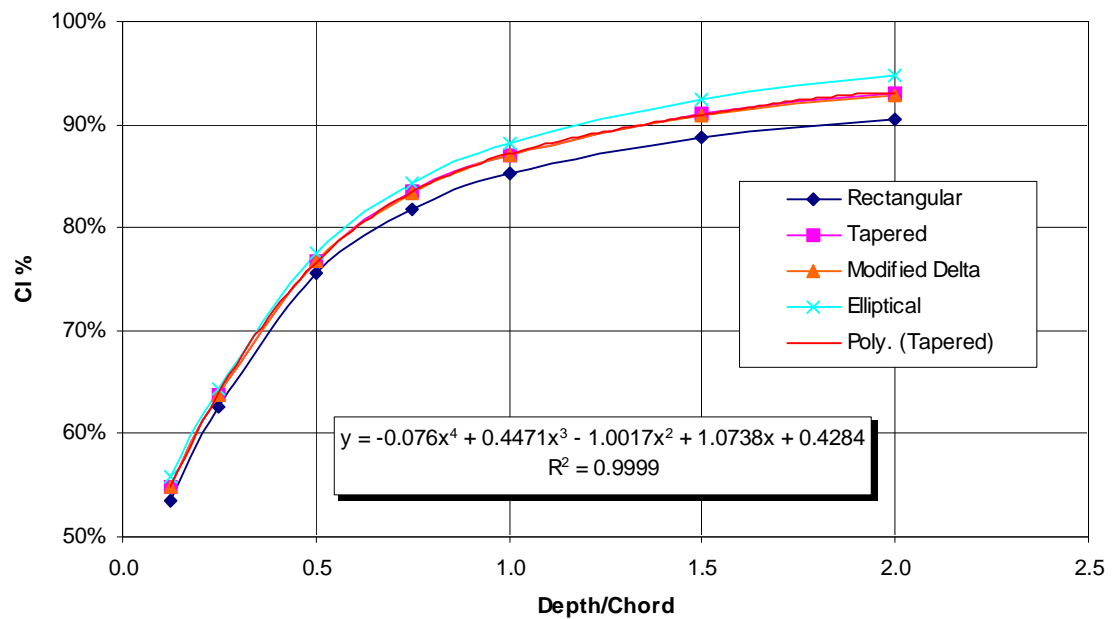
Figure 28   Percent change in lift coefficient vs. depth ratio.
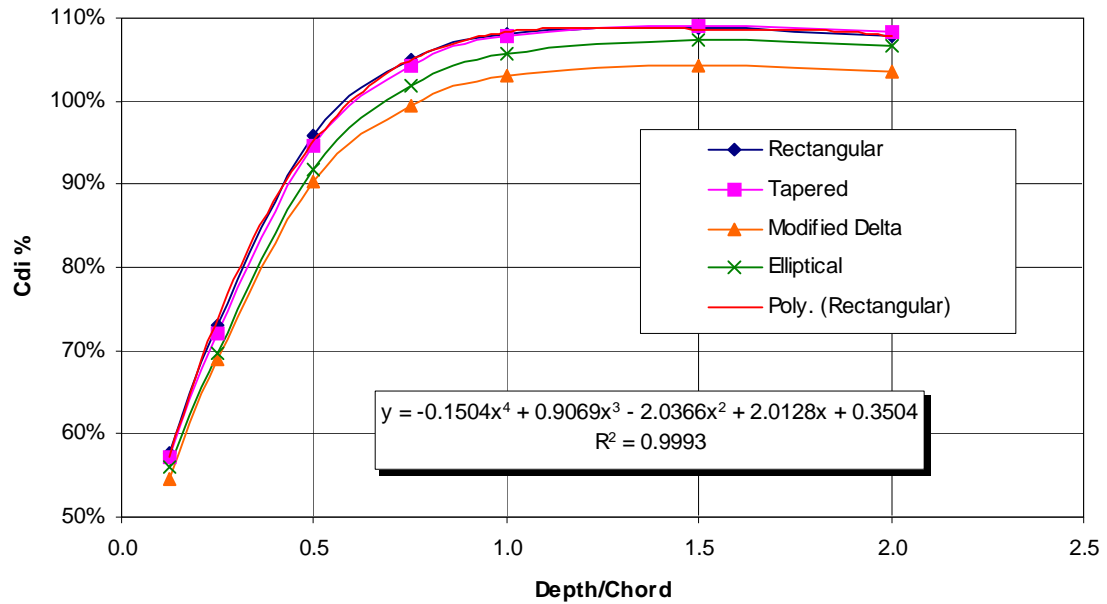
Figure 29   Percent change in induced drag coefficient vs. depth ratio.

$$\%C_L = -0.076d^4 + 0.447d^3 - 1.002d^2 + 1.074d + 0.428 \tag{29}$$

$$\%C_{Di} = -0.150d^4 + 0.907d^3 - 2.037d^2 + 2.013d + 0.350 \tag{30}$$

Where: $\%C_L$ = The percentage of the infinite depth lift coefficient

               $\%C_{Di}$ = The percentage of the infinite depth induced drag coefficient

               d = Depth below the free surface measured in chords.

Equations 29 and 30 are applicable for the range of operation (depth ratios) for the

particular designs that were considered in this project. Theoretically, both equations

should converge to 0.5 at a depth to chord ratio of 0.0. They are only valid to a minimum

depth to chord ratio of 0.125. At depths less than this, ventilation would ensue and the

basis of the calculations in Hy2Perf would become invalid. This particular numerical

boundary is not a hard coded stop flag in Hy2Perf and the user must be aware that broaching or ventilation are definite possibilities any time the depth to chord ratio reaches values below 0.125. Hy2Perf was subsequently modified to use equations 29 and 30 to adjust the lift and induced drag coefficients for free surface effects.

5 - HYBRID HYDROFOIL DESIGN AND EVALUATION

The development of a hybrid design that met the initial goals of this thesis was an iterative process. It involved changes in hull form philosophy, modifications to the software and the development of additional software to validate and improve the accuracy of the calculations. This section will provide the highlights of the developmental process, documenting the evolutionary forces that concluded with a design that met the initial criteria: a practical design that delivered improved performance at high speeds.

5.1 - Hull Design

The initial approach to this project was to strive for a performance improvement by simply setting a target. The lift to drag theories described in Section 1 were not fully developed until the performance evaluation was well underway. The initial design philosophy that was pursued was to reduce the drag contributed by buoyant lift to acceptable levels by substituting dynamic lift and its related drag factors only up to the point needed to achieve the performance goals. An arbitrary target of 50% buoyant lift and 50% dynamic lift was set and the initial hull forms were developed to support this philosophy.

The resulting hull design was a trimaran configuration that featured a bulbous bow on the main hull. Buoyancy was distributed so that 80% of the buoyancy at full load was provided by the center hull and 10 % by each of the amas. When operating at full speed, the hull "flew" at a height that reduced draft to approximately 50% of the static value. Figure 31 shows a wire frame image of the design.
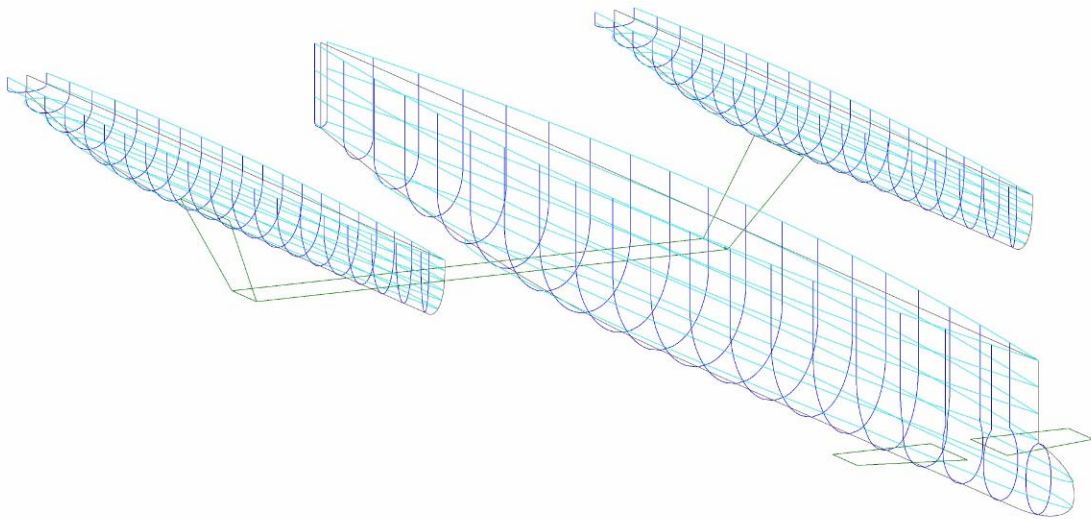
Figure 30   Initial hull design, Model A.

After reviewing the performance results for this design and considering the basic factors driving the L/D relationships, the work leading to the development of Equation 15 was undertaken. This equation and the results from the initial tests on the hull design shown in Figure 29 indicated that the design point that was selected, approximately a 50/50 division of lift between buoyancy and dynamics, yielded the minimum lift to drag ratio possible for a hybrid hydrofoil. In other words, the design point turned out to be the peak of the resistance "hump." Even though this point was not an optimum for the design, it still provided a significant reduction in overall resistance.

To improve the design and obtain the maximum possible lift to drag ratio available, Equation 15 indicated that the entire hull would have to be lifted out of the water and that 100% dynamic lift was required. Operating in this mode, the vessel would be able to attain the target design speed at the lift to drag ratio of the foils alone. Exceeding the

target L/D of 20 would then become an exercise in foil design. This meant that some changes in the foil and hull design philosophy would be required.

Since the hull would now be lifted fully out of the water, there was no need to have a bulbous bow to reduce resistance in the intermediate draft ranges. A vertical stem design, with a small radius forefoot was adopted. This kept the waterlines and water-plane area nearly constant throughout the transition to fully foil borne operation. The objective of this was to minimize the natural resistance hump of the main hull by steadily increasing the length to draft ratio while holding the length to beam ratio relatively con-stant through the transition to flight. Another change that was made was to the static draft of the vessel. The length and beam were increased in order to reduce the static draft. This was done to minimize the distance that the hull would have to travel vertically to be lifted out of the water. Figure 30 shows a wire frame representation of the hull form that was finally developed.
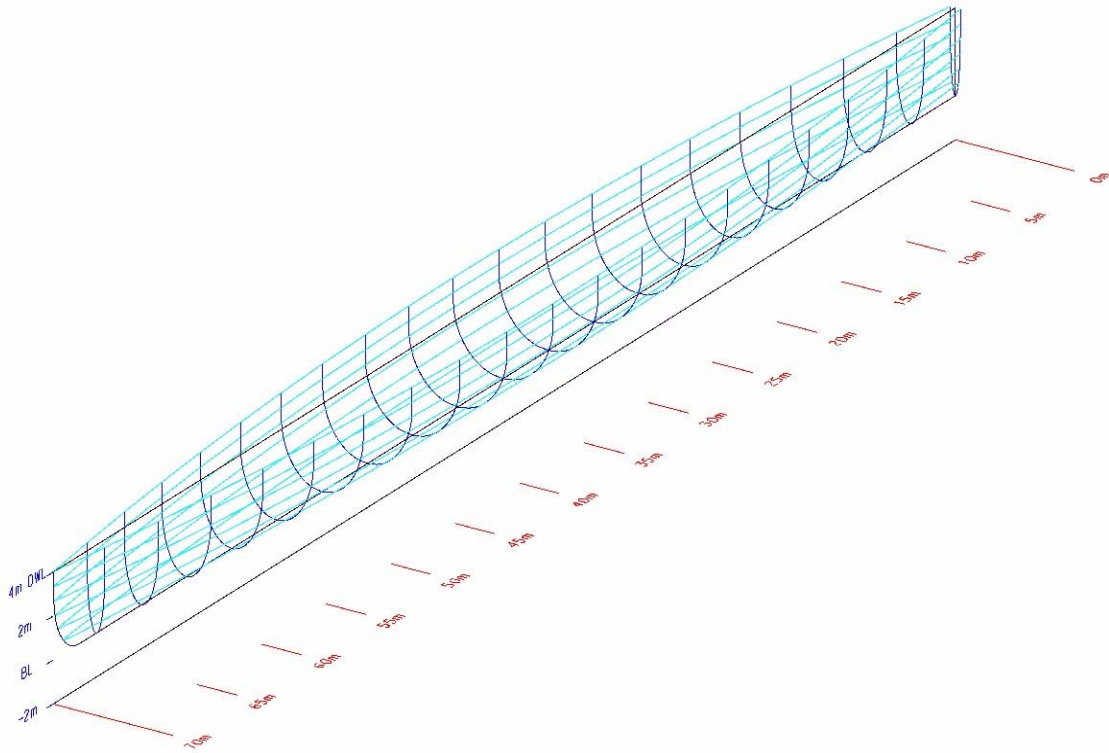
Figure 31   Center hull for the hybrid hydrofoil, Model B2.

5.1.1 - <u>Amas (outriggers)</u>

The amas used to stabilize the design at low speed were of a form similar to that

of the main hull. Some minor modifications were made to the transoms to minimize tran-

som wetting and low speed drag. The location of the amas relative to the center hull was

studied in detail for this project. The ultimate location was driven by several competing

factors. These included drag minimization, arrangements, and both transverse and longi-

tudinal stability.

Michlet allows the user to change the locations of the hulls of a multi-hull confi-

guration without reloading the hull offsets and parameter file, allowing for a rapid

assessment of location changes. It quantifies the effects by plotting the interference

forces between hulls for multi-hull designs on screen. These forces vary with speed,

changing from positive (advantageous) to negative (drag) at speeds below the point

where a transverse wave train is present. Two variables come into play in the placement

of the amas. The first is transverse spacing and the second is the longitudinal location of

the amas with respect to the center hull.

The transverse spacing of the hulls is the key factor in controlling interference ef-

fects. Locating the amas close to the center hull increases interference. Spacing them out

gradually reduces the interference to zero. It was found that a hull spacing of approx-

imately of the amas produced minimal interference. Only minor changes were seen in

the interference drag as the hulls were moved out to multiples of the waterline length.

The transverse spacing is ultimately limited by the properties of the materials used

to construct the vessel and the practicality of operating excessively broad beamed de-

signs. Transverse stability is usually adequate when the amas located at 50% of their

waterline length from centerline.

As with the transverse spacing, performance improved with a specific trend in the

longitudinal location of the amas. It was found that locating the amas aft of the midships

point on the main hull provided beneficial interference effects. Reductions in drag result

in any longitudinal placement of hulls that is aft of amidships with respect to the central

hull. Locating the amas forward of this point yielded detrimental results. Therefore, the

initial designs featured the hulls located in the most favorable position, as far aft as prac-

tical.

The concept of locating the amas aft, as shown in Figure 29, was abandoned as general arrangements were developed and cargo and fuel loading conditions were considered. The effect of fuel consumption on the longitudinal center of gravity (LCG) location was the primary driver in this decision. The Model A hull arrangement was a feasible design solution, but it would not accommodate large changes in displacement due to cargo or fuel load variations. It had a favorable LCG and static trim condition in only a limited number of loading conditions. This limitation posed some serious restrictions on the potential uses of the vessel.

In general, an arrangement that features an aft position for the amas is best suited for a vessel that experiences minimal changes in the location of the longitudinal center of gravity as fuel and cargo loads are changed. Such is the case for a short haul, high-speed ferry, where the fuel load can be minimized and the cargo would consist of lightweight, high volume items such as people and personal vehicles. Although not stated as a design criterion, this design concept is intended to be flexible enough to accommodate a wide range of applications and limiting it to a short haul role is neither appropriate nor necessary.

In order to maximize the range and cargo carrying capabilities of the design, a centralized position for the amas was adopted. By doing this, the longitudinal center of buoyancy was shifted to a location much closer to midships. The cargo deck and fuel tanks were subsequently located amidships as well. This modification allowed the vessel to maintain reasonable trim values under all loading conditions without ballast. Static

trim is a key factor in optimizing the L/D ratio of the hull and the foils at all speeds and will be discussed in the next section.

5.2 - Foil Design and Location

The foil design philosophy followed in this work was driven by achieving the highest lift to drag ratio possible. The primary factors in achieving a high lift to drag ratio are the aspect ratio of the wing and the design lift coefficient. Using Equation (8), an analysis of the maximum possible lift to drag ratios for wings was undertaken. Figure 31 shows the results of Equation (8) plotted for a range of aspect ratios. For each aspect ratio, it can bee seen that there is a peak efficiency point that is driven by the design lift coefficient of the wing. It also indicates that as aspect ratios increase, so to do the maximum L/D values. This information alone is insufficient for completing a foil design and other factors must be considered.
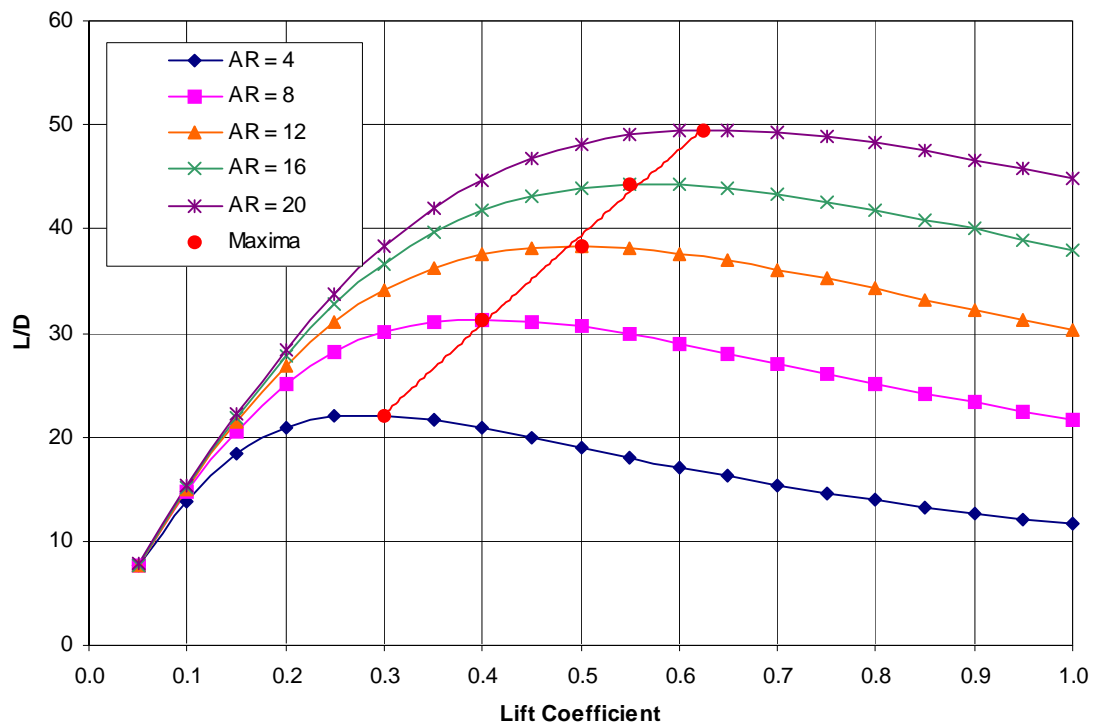
Figure 32   Lift to drag ratios of 3D wings in an infinite fluid (water).

Figure 31 indicates that an efficient hydrofoil should be designed with a high aspect ratio and a specific lift coefficient, which will result in the maximum efficiency for that aspect ratio. Additional factors that must be considered included pitch control, the practicality of large wing spans, the strength of the materials used in the foil construction, cavitation and flow separation. Cavitation and flow separation have direct impacts on the efficiency of the system as a whole and were considered during the foil design development.

Flow separation is difficult to predict and is directly related to the onset of cavitation. Without involving the use of additional software to test the limits of flow separation

and cavitation, a minimalist approach was adopted. The "rule of thumb" used for select-

ing propeller blade section lift coefficients is:

Do not to exceed a local lift coefficient of 0.4.[6]

Propeller sections, which are typically airfoil shapes, can normally operate with-

out the risk of cavitation or flow separation if their lift coefficients are kept below this

value. Using a design lift coefficient maximum of 0.4, Figure 31 indicates that a peak lift

to drag ratio greater than 40 could be achieved with an aspect ratio of 12. It also showed

that L/D values greater than 30 were possible for aspect ratios as low as 8. The selection

of the foil aspect ratio and span was thus bracketed between 8 and 12, with lift coeffi-

cients in the 0.3 to 0.4 range.

The secondary issue driving the foil design was pitch control. In order to develop

a practical, highly efficient foil system, the foils would have to be large and slender, ad-

justable to match varying load conditions and be self-stabilizing if possible. To achieve

this goal, a "tricycle" design approach was adopted. The main load would need to be car-

ried by a large high aspect ratio foil. Pitch and roll would be controlled by a smaller set

of foils or trim planes.[7] In order to achieve the highest lift to drag ratios possible for the

---

[6] Dr. William S. Vorus

[7] Roll stabilization was not explored in this study, but it is an eventuality that had to be considered. Using a

pair of trim planes allows for independent operation and subsequent control of both pitch and roll motions.

The alternatives include the use of surface piercing dihedral foils or control flaps. Both of these alterna-

tives introduced unnecessary technical complications.

vessel, all foils would be designed to develop their lift primarily from camber. This minimizes the risk of flow separation and simplifies the control of pitch.

Since the main lifting foil was designed for optimum performance at a particular installed angle of attack, it needed to be kept as close to that angle of attack as possible under all operating speeds. Trim planes were used to accomplish this task. However, their design and function had to include more than just pitch control. If the lifting load was dedicated 100% to the main foil, then the trim planes would be relegated to the task of just providing a trimming moment and their lift coefficients would be varied from +0.4 to –0.4 by changing their angle of attack. This turned out to be contrary to the objectives of the project.

Any surface that is placed into the water immediately inflicts a viscous drag penalty on the entire vessel. Since this design approach required trim planes for stability, they would have to operate at lift to drag ratios as close to the target L/D as possible. This meant that they would have to share a portion of the lifting load with the main foil. It also meant that in order to operate efficiently at the design speed and condition, they would probably operate in inefficient ranges during the transition to full flight and possibly in rough sea states.

The configuration of the main lifting foil and trim planes went through a number of iterations before arriving at the final design. The arrangement provided in Figure 32 shows two modified delta trim planes aft and a single modified delta foil forward. This arrangement provided the performance and load bearing flexibility needed to produce a design that met the original criteria for practicality as well as efficiency.
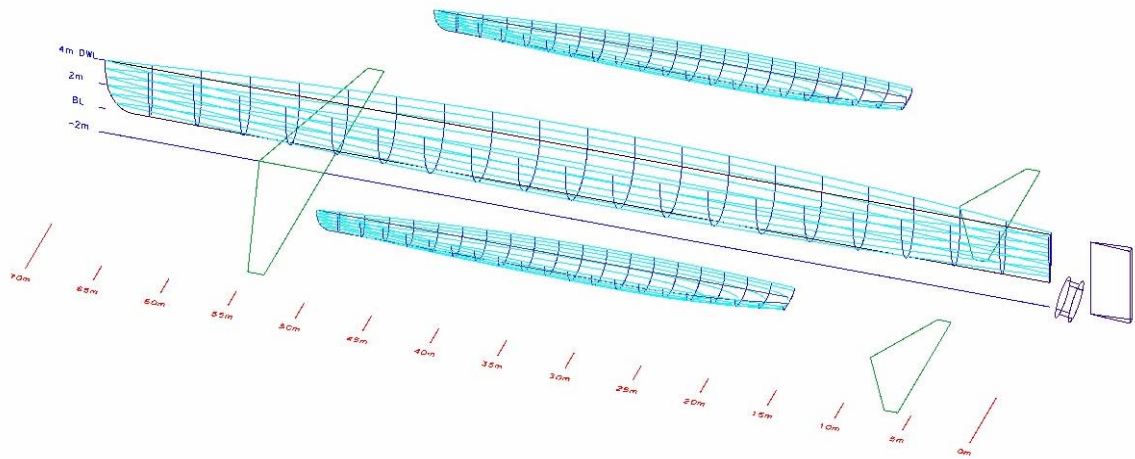
Figure 33   Model B2 hybrid hull lines and foil arrangement.

Additional considerations that were accommodated during this analysis and de-sign development included cavitation and structural concerns. Cavitation concerns were considered by use of the Brocket criteria of Equation 27. In order to insure that adequate foils could be designed, the thickness ratio was limited to at least 5% of the chord length. At velocities in excess of 25 m/s, with lift coefficients of 0.3 to 0.4, cavitation is indicated at any thickness over 5%. Tables 4 and 5 provide the design particulars for the hulls and lifting foils shown in Figure 32.

Table 4   Hybrid B2 hull characteristics.

	Main Hull	Amas	Ensemble
Length (m)	70.0	35.0	70.0
Max beam (m)	5.0	3.5	30.0
Transom Beam (m)	0.5	2.5	-
Depth (m)	4.0	1.5	4.0
Displaced Vol (m^3)	800.9	103.8	1,008.5
Wetted Area (m^2)	670.2	153.9	978.0
Length/Beam	14.0	10.0	2.3
Length/Depth	17.5	23.3	17.5
Block Coefficient	0.5721	0.5647	-
Prismatic Coefficient	0.6827	0.6884	-
Max Sect. Coefficient	0.8381	0.8202	-
Waterplane Coefficient	0.6829	0.7496	-

Table 5   Hybrid B2 hydrofoil characteristics.

	Main Foil	Trim Planes	Rudder
Cl	0.35	0.35	-
Cdb (cavity base drag)	-	-	0.009
Span (m)	27.0	12.0	6.0
Chord (m)	3.0	2.5	3.0
Area (m)	81.0	30.0	18.0
Aspect Ratio	9.0	4.8	2.0
t/c	0.05	0.05	0.10
Type	wetted	wetted	vented

5.3 - Performance Results

Results from the Hy2Perf performance calculations are shown in Figures 33 – 36.
Figure 33 shows the calculated resistances for the hybrid vessel with and without its hy-
drofoils. The calculations indicate that at the design speed of 25 m/s, which equates to a
Froude number of 0.95, the hybrid experiences a 44% reduction in resistance when it is

foilborne. When converted to terms of L/D, the hybrid vessel achieves a L/D of 11.6

when hullborne and a L/D of 26.2 when foilborne at 25 m/s. In order to provide a com-

parative analysis, the resistance data for a Series 62 Planing Monohull of equal

displacement was also included in the chart. It developed a L/D of 9.9 at the design

speed.
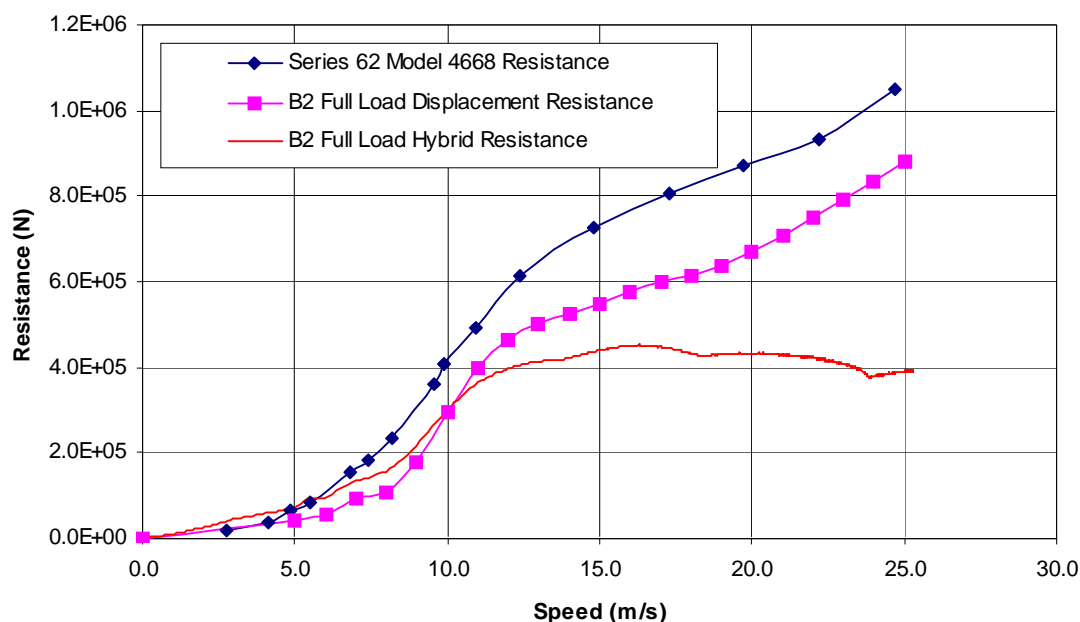
Figure 34   Hybrid hydrofoil full load resistance.

Figure 34 provides a reference for the changes in draft that the hybrid experienced

during the calculation. The drafts measured from the waterline to the keel at the forward

and aft perpendiculars are plotted in the figure. At the beginning of the run, there is ap-

proximately a 0.2m difference between the two drafts. The trim planes are able to

overcome this trim and zero the difference forward and aft by the time the vessel reaches

3 m/s (~ 6 kts.). At speeds above this, the trim planes are able to stabilize and maintain

the design trim throughout the transition to full flight. The chart indicates that the keel

cleared the surface of the water at a velocity of approximately 24 m/s and by the time the

vessel reached the design speed, the keel was approximately 0.5 meters above the water.
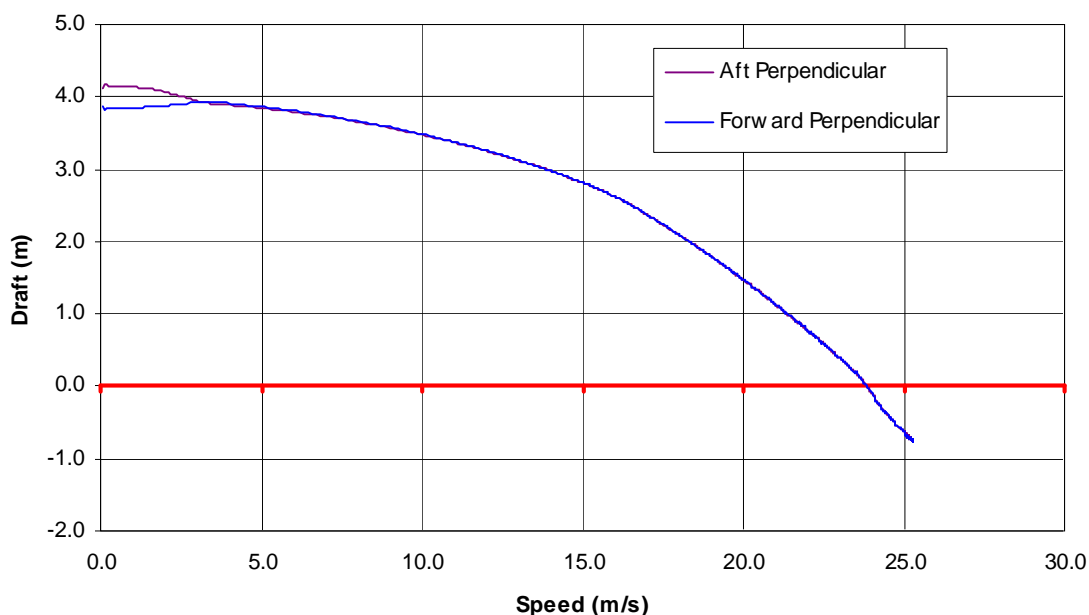
Figure 35   Hybrid hydrofoil draft vs. velocity.

Figure 35 is provided to show the amount of force needed to hold the vessel in a

zero trim attitude throughout the performance regime. It shows the trim plane angle of

attack versus the speed of the vessel. In order to avoid flow separation, the trim planes

were limited to +/- 8 degrees of total travel. When Hy2Perf detects that the craft is out of

trim, it increases or decreases the trim plane angle of attack until either the angle of attack

limits are reached or the craft is brought into trim limits. As the chart shows, the trim

planes were adjusted to their "stops" and held there until they were able to develop

enough lift to bring the craft into trim. This point is indicated where the angle of attack

reduces sharply from 8 degrees at a velocity of approximately 3 m/s. That point can be related to the point on Figure 34 where the forward and aft draft curves merged. The angle of attack for the planes decreases steadily as the craft speed increases and becomes fully foilborne.
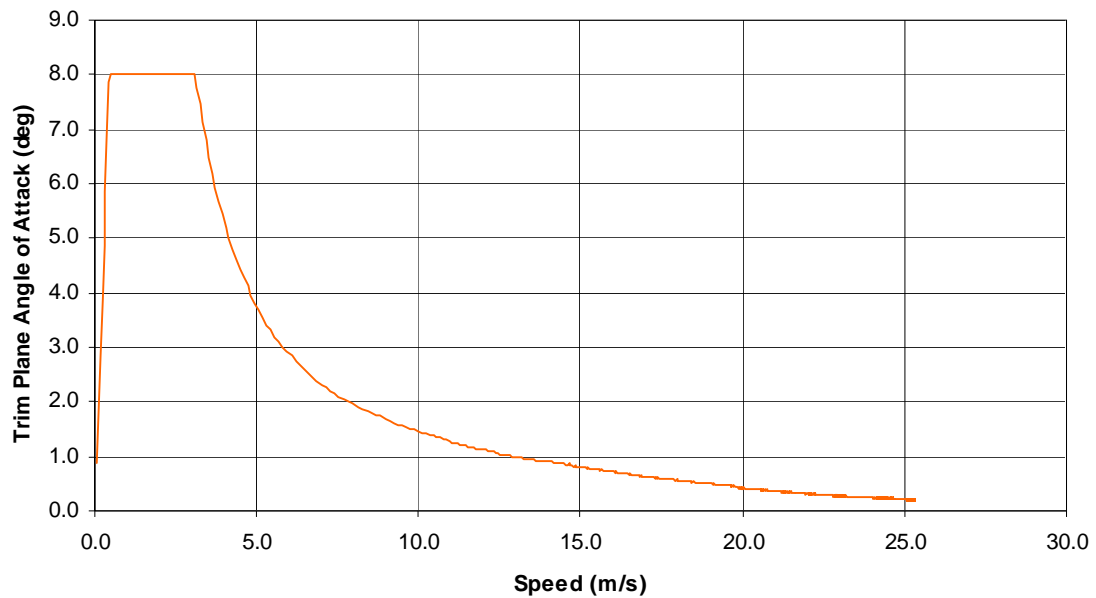
Figure 36   Hybrid hydrofoil trim plane angle of attack vs. velocity.

The design lift coefficient of the trim planes is 0.35 at the installed (ideal) angle of attack. The angle of attack indicated in Figure 35 includes the installed (ideal) angle of attack. In this case, that value is +0.54 degrees. The figure also shows that the trim plane design is well matched to the design load and speed conditions, since they stabilize at the design speed at the ideal angle of attack.

The data shown in Figures 33 – 35 was developed for a full load scenario. This included a full load of fuel and cargo. Additional calculations were made for a burned-

out (no fuel) condition to determine the effects of changes in displacement on the overall performance. Table 6 provides the weight estimate that was developed for the hybrid vessel. This particular weight estimate was developed for a trans-oceanic ferry. The distribution of weights is intentionally extreme in order to be conservative. A distribution of 50% craft weight, 40% consumables and 10% cargo was used. The object of this exercise was to determine the effects of fuel burn-off on the performance of the hull. Obviously, the distribution of weight between fuel, cargo and superstructure design can be varied with the mission and desired range of the vessel.

Table 6   Hybrid B2 weight estimate.

Description	Full Load	Burned Out
Main Hull	250,000	250,000
Amas	60,000	60,000
Focsle	10,000	10,000
Wet Deck	50,000	50,000
Deckhouse	50,000	50,000
Superstructure	30,000	30,000
Pilot House	5,000	5,000
Main Engine	25,000	25,000
Aux. Machinery P/S	20,000	20,000
Maneuvering Engines	20,000	20,000
Fwd Foil System	10,000	10,000
Aft Foil System	10,000	10,000
Fuel	410,400	22,800
Water	25,000	2,500
Vehicle Cargo (24 cars)	50,000	50,000
Passengers (200)	15,000	15,000
Total (kg)	1,040,400	630,300

Figure 36 provides the resistance data for the full load condition and the lightly loaded case after the fuel load is burned down to the margins. A significant difference in

total resistance is seen between the two load conditions at all speeds greater than 5 m/s. This test provided a number of noteworthy details. The most significant was that in order to keep the vessel operating at a foilborne height of less than one meter, power and speed must continuously be reduced as fuel burns off. The main lifting foil's angle of attack is presumed to be fixed, giving it a constant lift coefficient. As the fuel burns off, the total amount of lift required to fly the hull clear of the water decreases. If a constant height is to be maintained throughout the voyage, speed must be reduced to match the decreased demand for lift. By the end of the voyage, a speed of 20 m/s was the maximum possible.
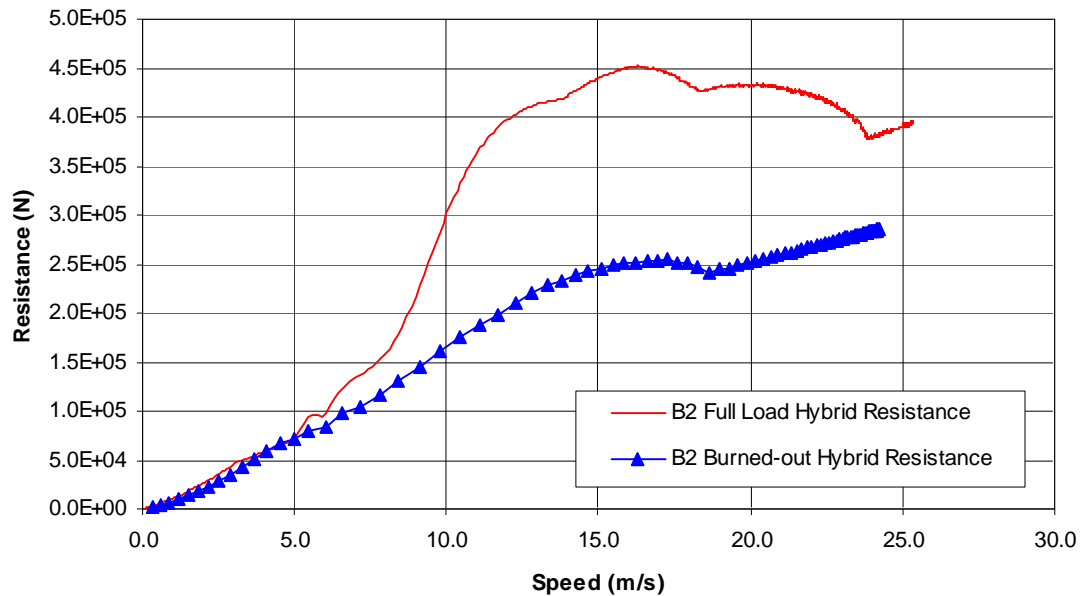

Figure 37   Hybrid hydrofoil resistance at full and lightly load conditions.

Using the data developed for Figure 36, a rough estimate of the range of the vessel was made. If both power and speed are reduced linearly throughout a voyage, their values and the fuel consumption rates for the full and burned out conditions can be aver-

aged. An estimate based on fuel consumption data published for the GE LM-1600 gas turbine and the presumption that a constant overall propulsive coefficient of 0.67 was attainable at all speeds was then made.

During the theoretical voyage, the average speed was 44 knots and the fuel supply was estimated to last for approximately 170 hours. This yielded a range of approximately 7,500 nautical miles. This range is more than enough for trans-oceanic service[8] and indicates that either light ship weight or the weight of additional cargo can be substituted for fuel.

Figure 37 shows the thrust curve used for the full load calculations. Also shown are the theoretical thrust and propulsive efficiencies that would result if the LM-1600 was used as the prime mover for this vessel.

---

[8] Key trans-oceanic ranges: San Francisco to Yokohama – 4,600 nm; New York to Le Havre – 3,200 nm; New York to Cape Town – 6,800 nm.
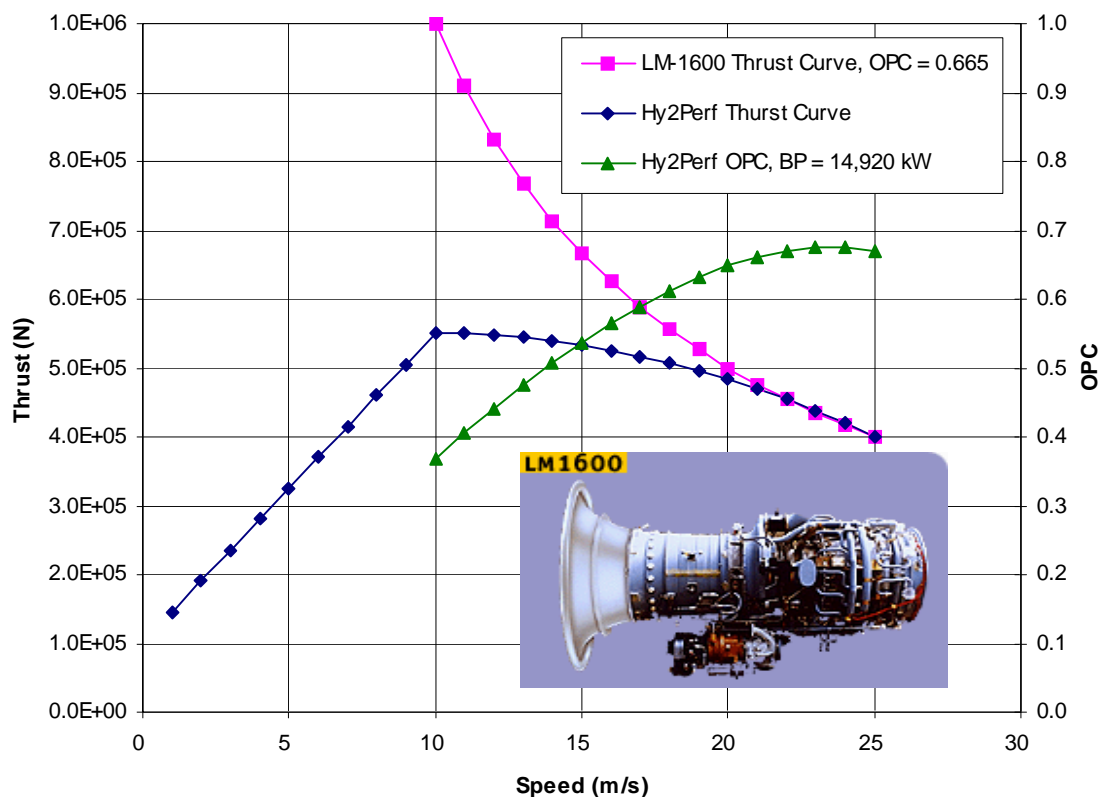
Figure 38   Conceptual propulsion system thrust characteristics.

5.4 - Practical Design Considerations

Thus far, discussions have been mainly concerned with the prediction of performance and the tools needed to make that prediction. Once the tools were in place, a number of factors concerning the practical aspects of the hybrid's design had to be considered. In Sections 5.1 and 5.2, a thorough discussion concerning the requirements for a practical hull and foil arrangement were undertaken. The decisions resulting from the factors discussed in these sections led to the performance characteristics provided in Sec-

tion 5.3. What is yet to be discussed is the method for achieving this performance.

cifically, how is the thrust developed and is it manageable under all conditions?

5.4.1 - Propulsion Systems

The main propulsion system for the hybrid consists of a single prime mover. At

this time, a suitable candidate for developing adequate power appears to be the GE LM-

1600 marine gas turbine. Proving that the torque produced by this engine can be turned

into thrust at the efficiencies indicated in Figure 35 is a task for the future. At this time,

the most likely candidate propulsor appears to be a counter-rotating surface piercing pro-

peller assembly. Although propellers of this type that are capable of absorbing the

20,000 BHP developed by the LM-1600 have not been designed to date, similar, smaller

ones have been developed and patented. Patent 5,230,644, assigned to the Brunswick

Corporation details the design of what is now marketed as the Blackhawk^{TM} counter-

rotating surface drive. A picture of one of these propeller assemblies appears in Figure

38.

Figure 39   Counter-rotating surface piercing propeller.

A propeller configuration similar to this would be ideal for the hybrid hydrofoil for two reasons. First, it would allow the propeller to be mounted at a shallow angle, positioning the hub approximately 1 meter below the baseline of the center hull. When the hull is flying at its optimum height, the propeller would be submerged to its optimum depth. This installation would help control the height of the hydrofoil above the water because thrust would begin to decrease rapidly as the propeller emerges from the water. This makes broaching in calm water due to excessive speed very unlikely.

The second advantage of the counter-rotating arrangement is that the horizontal component of thrust created by a conventional surface drive is not present. If such a drive were to be used, a continuous offsetting force would have to be provided by the rudder. This would lead to a decrease in overall efficiency.

The high-powered prime mover cannot be relied upon for all situations. The main shortcoming of this power plant is that it is ineffective for low speed operations and maneuvering. The surface drive will not operate efficiently when it is fully submerged and although it is a twin screw assembly, it functions like a single screw when maneuvering.

Maneuvering requirements and the possibility of low speed operations due to severe weather or other causes dictate that the hybrid possess an efficient low speed propulsion system as well as the high-speed prime mover. The ideal maneuvering propulsor would be one that is either diesel or electric and could be mounted on the amas. This location provides maximum leverage for maneuvering.

Searches of possible alternatives lead to the discovery of a suitable candidate propulsor. Schottel, Inc. manufactures a series of retractable drive units as well as propulsor

assemblies (Figure 39) to mount on the units. These propulsors could be mounted port and starboard on the amas. They would be raised out of the water for high-speed operations and lowered for maneuvering and low speed operations. The amount of power selected for these units would depend on the maximum speed desired during hullborne operations. A number of commercially available high-speed marine diesels would be suitable for this purpose.

Figure 40   Low speed and maneuvering thruster.

5.4.2 - Foil Retraction

The hydrofoils that the hybrid would be equipped with must be kept in good condition at all times in order to produce the designed lift to drag ratios. The foils must be kept free of debris and marine growth, in order to minimize drag and maintain lifting cha-

racteristics. In the event of a collision with a submerged object or large marine animal, the foils must be easy to repair or replace. These are just a few of the factors that dictate that the hybrid should be equipped with retractable foils.

A foil retraction system also allows the craft to operate as a pure trimaran and take advantage of lower drag by reducing the wetted surface area added by the hydrofoils. Additionally, it reduces the risk of damage to the foils during docking and maneuvering in confined spaces and shallow water.

The concept foil arrangement would have the foils mounted on individual struts, which would hinge parallel to the centerline of the craft. The trim planes are located aft of the amas and could be rotated up and clear of the water without interference. In order to retract the bow foil using this method, it would have to be split at the centerline and it would have to be mounted forward of the amas. Each half of the foil could then be arranged to fold up in a similar manner as the trim planes. The main foil halves would have to be positively coupled when deployed, so that they form a continuous span.

5.5 - Concept Arrangement

The following figures detail a concept arrangement for a hybrid hydrofoil. This arrangement depicts the vessel in a configuration that conforms to the weight estimate shown in Table 6. It is strictly conceptual and is intended to show the hull form, propulsion system and hydrofoils with a conceptual topside arrangement. Since the performance calculations did not take aerodynamic drag into effect, the performance shown in the previous sections can be expected to be influenced by the presence of a

large superstructure. This same hull and main deck arrangement can easily be used to develop a container ship or combatant vessel.
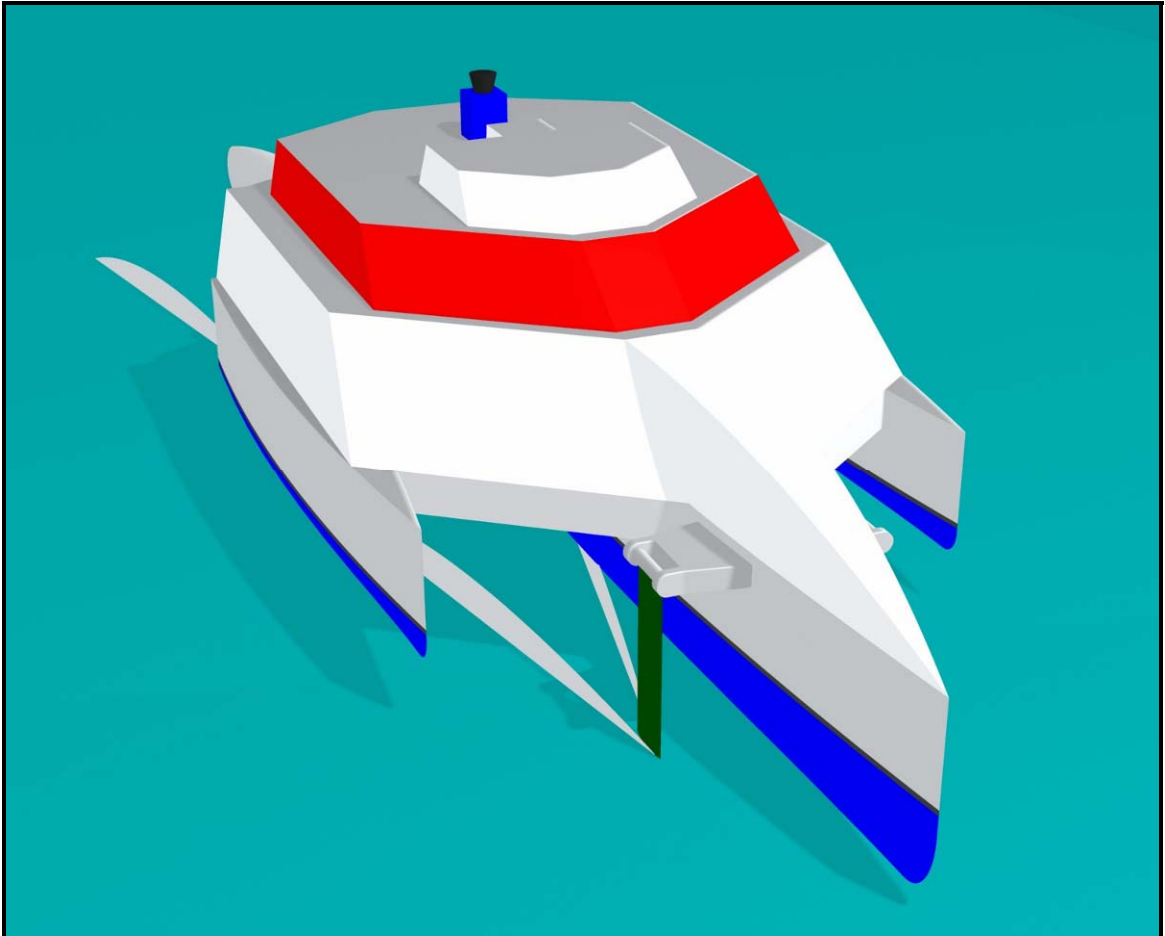

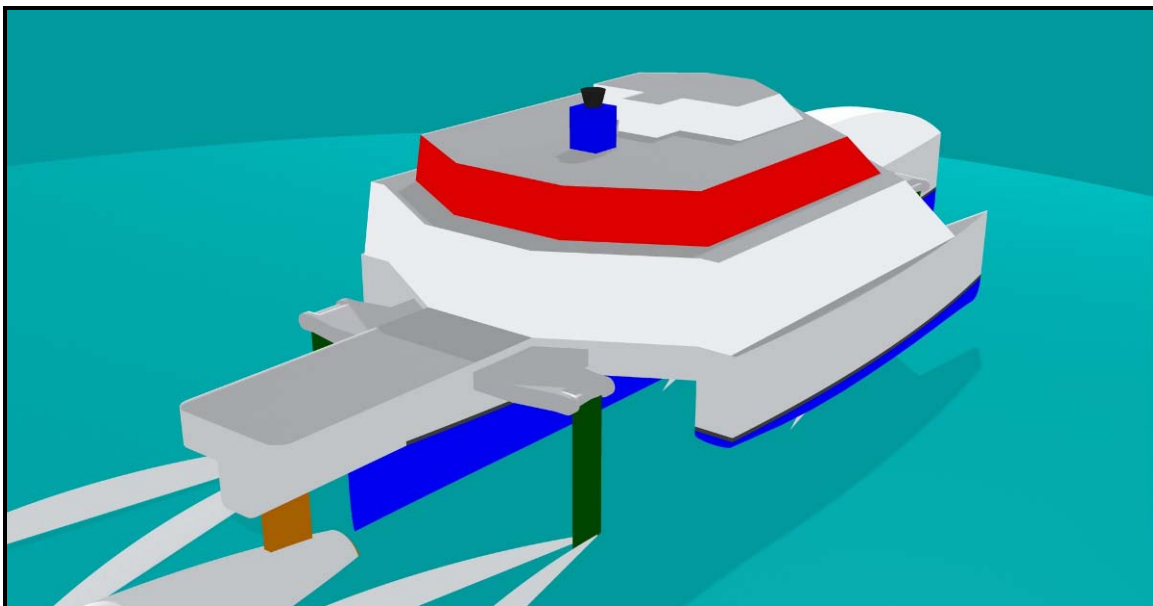Figure 41   Hybrid hydrofoil concept, forward quarter view, foilborne.

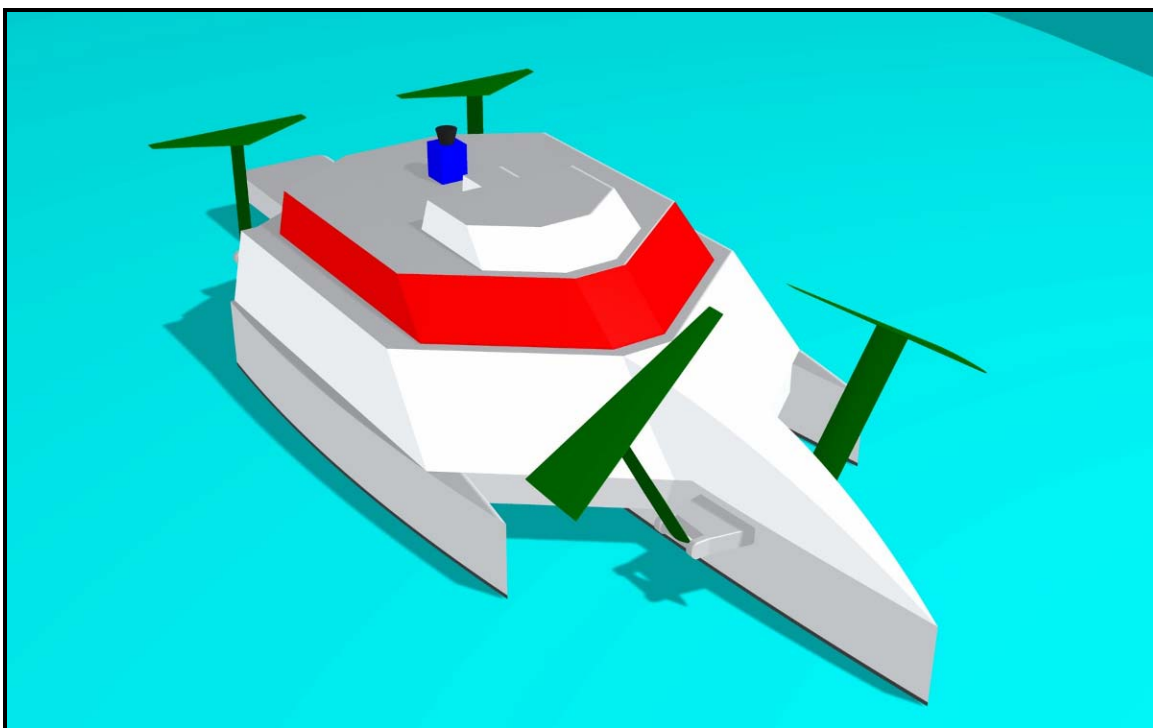Figure 42   Hybrid hydrofoil concept, aft quarter view, foilborne.

Figure 43   Hybrid hydrofoil concept, forward quarter view, hullborne.

6 - CONCLUSION

6.1 - Objectives Met

In its essence, the primary objective of this work was to show that it is possible to reduce the overall resistance of a high speed surface vessel by exchanging the wave making and viscous drag associated with buoyant lift for lesser amounts of induced and viscous drag associated with dynamic lift. To guide the process and produce a useable product, specific goals were set. These included the following items:

1. Develop a design that is capable of high speeds.

2. The resulting design must have resistance characteristics superior to other vessels currently in service. (L/D >= 20, Fn $\approx$ 1.0)

3. The design must be practical with respect to manufacturing and operational demands.

All of these objectives have been achieved. To accomplish this, a number of numerical analysis tools were used to both test the theory and produce the concept design. These tools were validated and then used to produce a "first order" approximation of the performance of the hybrid, confirming the hypothesis.

The design that was produced is capable of high speeds. The calculations show that a design speed of 25 m/s (48.6 knots), which fits the definition of high speed established in Section 1, is possible. Although this speed represents a Froude number of 0.95 for the concept design, the craft would be capable of achieving the velocity required to exceed 1.0. The design lift to drag ratio exceeded the target by 30%. These achieve-

ments should be tempered with the knowledge that aerodynamics and parasitic drag from struts will reduce the L/D somewhat.

The design is arguably practical. Discussions concerning the practicality of developing the required thrust and maintaining the foil system were provided in Section 5. Even though the discussions concerning the structural design and construction feasibility were not fully developed, the concept hull form is not radically different for a number of designs in service today. These include high-speed catamarans, surface effect ships, hydrofoils and trimarans. With this in mind, the development of a hull structure that meets the strength and weight requirements is possible.

6.2 - Unexpected Results

A number of unexpected results emerged from this work. The most significant is the development of the rough order of magnitude formulas used to predict the maximum lift to drag ratios of surface vessels. At the outset of this work, this author understood only the viscous friction equation for a displacement vessel (Equation 7). As the work progressed, additional questions were raised concerning the L/D relationships for a lifting surface and an air cushion vessel. Eventually, these relationships and the methods for combining them to predict the performance of hybrids were understood. The resulting formulas provide a useful tool for evaluating initial requirements and establishing realistic limits on performance.

Other unexpected results dealt with the specifics of the hybrid hydrofoil's performance. The most surprising of which was that the initial design philosophy of only partially supporting the craft with dynamic lift yielded minimum, not maximum, results.

This was discovered as the formulas for the L/D of a hybrid hydrofoil were being developed and lead to the "full flier" concept proposed in Section 5.

Additional items included the development of an understanding of effects of the main foil's chord and its location below the keel, on the vessel's stability as the hull broaches during take-off. Since the lift of the foil is affected by the presence of the free surface, the depth to chord ratio should be less than 1.0 when take-off occurs. If it is not, positive lift control is needed for the main foil because as the hull broaches, the vessel will experience a sudden reduction in drag and an increase in speed and lift. If the foil is too deeply submerged, these compounding effects will launch the boat and foils out of the water before the free surface can have an influence or thrust can be reduced.

6.3 - Issues To Be Resolved

During the course of this project, several issues arose that could not be fully addressed within the time allotted. These issues had no affect on the validity of the performance prediction, but they do raise questions about the practicality of the design. They fall into two main categories, safety and feasibility.

The safety of hydrofoils has been in question for a number of years. The primary danger to hydrofoils comes from collisions with shallowly submerged objects. These include marine life, natural debris, fishing gear, dunnage and even cargo containers. Two approaches could be taken to mitigate these risks. Either build the foils to break away in the event of a collision or build them to be as close to unbreakable as possible. Both of these approaches have their drawbacks. Breakaway foils may break away in high sea

states and bulletproof foils might be too bulky and heavy to produce the required performance.

The concept proposed in this thesis hopes to mitigate the dangers associated with a collision by keeping the hull as close to the water as possible. Should a foil failure occur, this craft would not fall less than one meter before lift is restored by buoyancy. This should reduce the danger of a rapid deceleration associated with hydrofoil and air cushion vessel "plow-ins."

The retractable foil system does much to reduce feasibility concerns. Obviously, one would not expect to be replacing foils after each voyage, but the foil system could be designed with "weak links" that would limit damage to the struts, allowing the foils to break away cleanly in the event of a collision. This would simplify replacement and possibly permit recovery and repair of the parted foil.

The final feasibility concern deals with seakeeping. All of the performance analysis done in this work presumes "first order" responses and flat seas. The concept of flying the hull with a minimum air gap leads to the assumption that in any sea state that exceeds the air gap, portions of the hull will be intermittently wetted. As sea states increase, a greater and greater percentage of the keel and hull bottom will be wetted. This increase in wetted surface area will have an adverse effect on the viscous drag and subsequently reduce speed. The maximum sea state that this concept can fly in is an unknown. To mitigate the danger of becoming stranded when high seas are encountered, a low speed propulsion system is proposed. This, combined with a stable, seaworthy hull form,

helps minimize safety concerns, but does not provide assurances that the concept is ultimately commercially feasible for ocean service.

6.4 - <u>Further Investigation</u>

As with any research project, the results of this work are not entirely conclusive. However, it does provide strong evidence that efficient hybrid hull designs are possible and that these hybrids are capable of delivering significant improvements in efficiency at high speeds. Ultimately, prototype testing of the hybrid hydrofoil concept will be required to verify the performance predictions made in this thesis and to ascertain whether any of the safety or feasibility concerns are insurmountable. Further investigation into the hybrid hydrofoil concept is definitely warranted. In addition, more effort should be devoted to verifying and enhancing the elementary L/D equations that have been proposed. This work should include experimental verification, expansion to include aerodynamic effects, and finally, the inclusion of significant second order drag factors.

REFERENCES

[1]   Beck, Robert F. 1989. Ship Responses to Regular Waves. *Principles of Naval Architecture* Vol. 3, Ch. 8, Sect. 3. Jersey City, NJ: The Society of Naval Architects and Marine Engineers.

[2]   Breslin, John P.; and Andersen, Poul 1994. *Hydrodynamics of Ship Propellers.* Cambridge, U.K.: Cambridge University Press.

[3]   Brocket, T. 1966. *Minimum Pressure Envelopes for Modified NACA-66 Sections with NACA a=0.8 Camber and BUSHIPS Type I and Type II Sections.* DTMB Report Number 1780. Washington: Bureau of Ships.

[4]   Clement, E.P.; and Blount, D.L. 1963. Resistance Tests of a Systematic Series of Planing Hull Forms, *Transactions of SNAME* 71:491-579.

[5]   Havelock, T.H. 1928. Wave Resistance. Proce*edings of the Royal Society of London*. Series A, Vol. 118:24-33.

[6]   Katz, Joseph; and Plotkin, Allen. 1991. *Low-Speed Aerodynamics From Wing Theory to Panel Methods.* New York: McGraw-Hill.

[7]   Lazauskas, L. 2000. *Michlet 6.06 User's Manual*.

[8]   Lee, Choung M.; and Curphey, Richard M. 1977. Prediction of Motion, Stability, and Wave Load of Small-Waterplane-Area, Twin-Hull Ships, *Transactions of SNAME* 85:94-130.

[9]   Michell, J.H. 1898. The Wave Resistance of a Ship. *Philosophical Magazine*. Series 5, Vol. 45:106-123.

[10]   Newman, John N. 1977. *Marine Hydrodynamics*. Cambridge Mass., The MIT
        Press.

[11]   Tuck, E.O. 1987. *Wave Resistance of Thin Ships and Catamarans*. Report T8701.
        Applied Mathematics Department, the University of Adelaide.

[12]   Wadlin, Kenneth L.; and Christopher, Kenneth W. 1958. *A Method for Calcula-
        tion of Hydrodynamic Lift for Submerged and Planing Rectangular Lifting
        Surfaces.* NACA Technical Note 4168. Washington: National Advisory Commit-
        tee for Aeronautics.

[13]   Wadlin, Kenneth L.; Shuford, Charles L. Jr.; and McGehee, John R. 1952. *A
        Theoretical and Experimental Investigation of the Lift and Drag Characteristics
        of Hydrofoils at Subcritical and Supercritical Speeds.* NACA Report 1232. Lang-
        ley, VA: National Advisory Committee for Aeronautics.

[14]   Yeh, Hugh Y.H. 1965. Series 64 Resistance Experiments on High-Speed Dis-
        placement Forms, *Marine Technology* Vol.2, No. 3:248-272.

[15]   Various authors. 1967. *Small Craft Data Sheets*. SNAME Publication D-13

APPENDIX A – HULLGEN (FORTRAN PROGRAM)

```
Code deleted to reduce file size.  If you would like a copy of
the codes used in this project, e-mail me at
ken.maloney@gmail.com
```

APPENDIX B – MULTIHYD (FORTRAN PROGRAM)

```
Code deleted to reduce file size.  If you would like a copy of
the codes used in this project, e-mail me at
ken.maloney@gmail.com
```

APPENDIX C – HY2PERF (FORTRAN PROGRAM)

```
Code deleted to reduce file size.  If you would like a copy of
the codes used in this project, e-mail me at
ken.maloney@gmail.com
```

APPENDIX D – LIFTLINE (FORTRAN PROGRAM)

```
Code deleted to reduce file size.  If you would like a copy of
the codes used in this project, e-mail me at
ken.maloney@gmail.com
```

APPENDIX E – COMMON CODE (FORTRAN SUBROUTINES)

```
Code deleted to reduce file size.  If you would like a copy of
the codes used in this project, e-mail me at
ken.maloney@gmail.com
```

VITA

Kenneth Maloney was born on November 16, 1956, in Corpus Christi, Texas. He was graduated with the class of 1974, from Archbishop Shaw High School in Marrero, Louisiana. In 1991, Kenneth enrolled in the School of Naval Architecture and Marine Engineering at the University of New Orleans. He completed the undergraduate program in 1998, obtaining B.S. degree in Naval Architecture and Marine Engineering. He subsequently enrolled in the Graduate School at UNO and continued his studies in naval architecture, focusing on hydrodynamics.

Kenneth became interested in naval architecture shortly after leaving high school. He began a career in shipbuilding in 1978, working as a draftsman. This eventually led to positions of greater responsibility in engineering, manufacturing and management. His experiences in shipbuilding exposed him to both high and low speed designs build for a variety of purposes including commercial, military and private applications.

Kenneth was employed by TEXTRON Marine and Land Systems, a division of TEXTRON, Inc., and worked full time at its New Orleans shipyard while studying for his graduate and undergraduate degrees. He joined the Society of Naval Architects and Marine Engineers in 1995 and was awarded the Society's Tommy L. Richards Scholarship in 1999.